AD NUMBER

AD450558

NEW LIMITATION CHANGE

TO

Approved for public release, distribution unlimited

FROM

Distribution: No foreign

AUTHORITY

RSIC ltr., 3 Feb 1966

ARPA ORDER NO. 347

PROJECT CODE NO. 7400

GENERAL MOTORS CORPORATION

TECHNICAL REPORT

ON

BODY SHAPE EFFECTS ON AXISYMMETRIC WAKES

Sponsored By

ADVANCED RESEARCH PROJECTS AGENCY

Monitored By

U.S. ARMY MISSILE COMMAND

CONTRACT NO. DA-01-021-AMC-11359(Z)

HYPERVELOCITY RANGE RESEARCH PROGRAM

A PART OF PROJECT "DEFENDER"

GM DEFENSE RESEARCH LABORATORIES

SANTA BARBARA, CALIFORNIA

AEROSPACE OPERATIONS DEPARTMENT

TR64-02K

OCTOBER 1964

450558

ARPA ORDER NO. 347

Copy No 1[illegible]

PROJECT CODE NO. 7400

GENERAL MOTORS CORPORATION

TECHNICAL REPORT

ON

BODY SHAPE EFFECTS ON AXISYMMETRIC WAKES

BY

L.N. WILSON

THIS RESEARCH WAS SUPPORTED BY THE
ADVANCED RESEARCH PROJECTS AGENCY
AND WAS MONITORED BY THE
U.S. ARMY MISSILE COMMAND
REDSTONE ARSENAL, ALABAMA

GM DEFENSE RESEARCH LABORATORIES

SANTA BARBARA, CALIFORNIA

AEROSPACE OPERATIONS DEPARTMENT

CONTRACT NO DA-01-021-AMC-11359(Z)
HYPERVELOCITY RANGE RESEARCH PROGRAM
A PART OF PROJECT "DEFENDER"

TR64-02K

DDC AVAILABILITY NOTICE

Qualified requesters may obtain copies of this report from DDC

OCTOBER 1964

FOREWORD

This report is one of a series of related papers covering various aspects of a broad program to investigate the flow-field variables associated with hypersonic-velocity projectiles in free flight under controlled environmental conditions. The experimental research is being conducted in the Flight Physics Range of GM Defense Research Laboratories, General Motors Corporation, and is supported by the Advanced Research Projects Agency under Contract No. DA-01-021-AMC-11359(Z). It is intended that this series of reports, when completed, will provide a background of knowledge of the phenomena involved in the basic study and thus aid in a better understanding of the data obtained in the investigation.

ABSTRACT

Experimental measurements have been made of the distance of transition to turbulence of the wake behind hypersonic spherical and blunted-cone models at hypersonic speeds in a ballistic range. Transition distances behind blunt bodies were found to be independent of body shape, whereas a definite shape effect was observed for slender bodies. A single shape parameter was determined which successfully correlated all the slender body data. The transition process was found to be markedly different between blunt and slender body flows, the transition occurring rather abruptly behind blunt bodies and being extended over many body diameters for slender bodies. In all cases, the transition distances were independent of body size and flight speed. The correlations were found to break down at high Reynolds numbers where turbulence originated at the recompression region. A method of using the distance to transition in clean wakes to discriminate between blunt and slender bodies is outlined.

CONTENTS

ILLUSTRATIONS

LIST OF SYMBOLS

a	speed of sound
b	wake diameter
c_R	disturbance phase speed, relative to wake edge speed
C_{Df}	boundary layer drag coefficient based on free-stream conditions and base area
C_{Dp}	pressure drag coefficient based on free-stream conditions and base area
D	model diameter
M	Mach number
p	pressure
Re	Reynolds number per unit length, $Re = \frac{\rho V}{\mu}$
S	shape parameter defined by Equation 2
T	temperature
V	model speed
w_c	wake speed (relative to wake edge) where gradient of density-vorticity product vanishes
x	transition distance measured from model nose
Γ	free-stream density in atmospheres $\Gamma = \rho/\rho_o$
μ	fluid viscosity
ρ	fluid density
ρ_o	standard sea level density

SUBSCRIPTS

e	conditions at wake edge
o	conditions on wake centerline
∞	free stream (ambient) conditions

I INTRODUCTION

Present methods of detecting and discriminating among various reentering vehicles rely upon observables which are characteristic of the vehicle's shape, speed and altitude. The trail deposited by vehicles within the atmosphere is a source of such observables, and as such has been the subject of much scientific interest in recent years. In particular, the striking differences between the near-wake signatures of blunt and slender body shapes suggest a possible means of discrimination.

Blunt-body wakes are characterized by a high-temperature inviscid outer wake (Figure 1) generated by the strong portion of the detached shock at the body nose, and a high-temperature, but narrow viscous inner wake generated by the body boundary layer. In the case of a slender body, this inner wake becomes much more important because of thicker boundary layers developed on the body and also because the inviscid wake is at a lower temperature, being generated by a weaker body shock. Consequently, the radiation and electron observables generated in the trail vary from a case in which the flow field is shock-dominated to one in which it is boundary-layer-dominated as the body becomes more slender.

Further, the transition of the laminar viscous wake to turbulence is shape-dependent, inasmuch as wake stability is governed largely by the temperature difference between the inner and outer wake. The location of the onset of turbulence is of prime importance both as an observable per se and because turbulence mixing radically affects the observables. If the trail of a hypersonic vehicle is to be used as a means of discrimination between blunt and slender bodies, a systematic study of shape effects is essential.

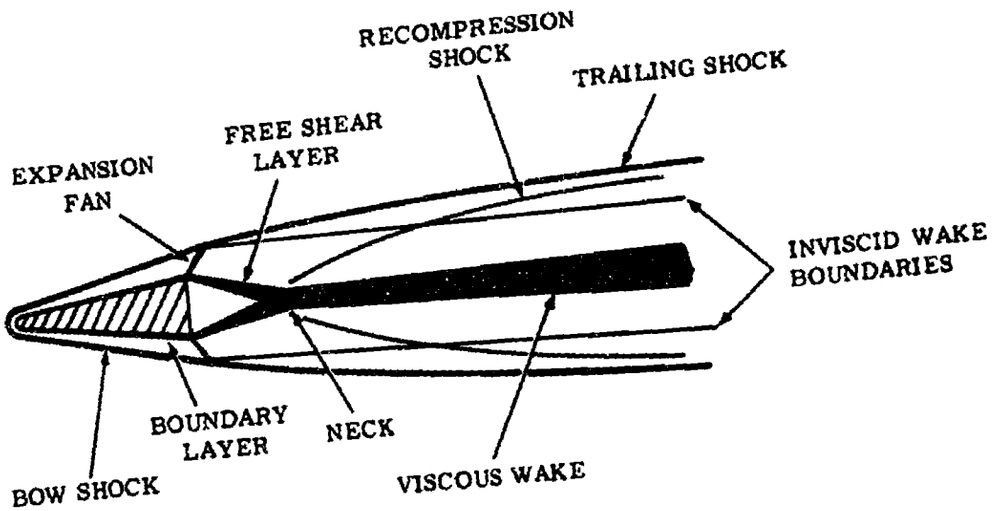

Figure 1 Sketch of Flow Field about Hypersonic Blunted Cone

Earlier measurements of observables obtained in the GM DRL Ballistic Range have been reported elsewhere.[1, 2]* The present paper is concerned with schlieren studies of the laminar trail and transition to turbulence.

II BACKGROUND

Experimental evidence[3] indicates that the transition process in two-dimensional viscous wake flows can be classified into three sequential regions: a linear, a nonlinear and a three-dimensional region. It is expected[4] that transition behind three-dimensional, axisymmetric bodies will be of a similar nature.

The first instabilities observed are small sinusoidal oscillations corresponding to the classical Tollmein-Schlichting type. These oscillations amplify exponentially in the linear region, eventually becoming finite, nonlinear waves in the nonlinear region. The nonlinear disturbances appear to be vortical in nature, being best explained by a model which consists of a double row of two-dimensional vortices, analogous to the classical Kármán vortex street. These vortices subsequently distort into three-dimensional disturbances before finally breaking up into three-dimensional turbulence.

Experimental observations have been limited to a large extent to the location of transition as determined by the first evidence of disturbances in the laminar wake (the beginning of the linear region), since it is here that the flow first becomes unstable. Further reference in this paper to the transition point will imply such a definition.

It is expected that the location of the transition point is controlled largely by a Reynolds number based upon local wake conditions. At extremely low Reynolds numbers, instabilities which might occur are damped by viscous dissipation placing a lower limit on the Reynolds number at which transition may occur. As the Reynolds number increases, the transition point moves towards the body

* Raised numbers in parentheses indicate references, listed at the end of this report.

until, in the vicinity of the body, it becomes "lodged" at the "neck" (Figure 1). Since the free-shear layer formed by the boundary layer separating from the base of the body is stable at high Mach numbers, the transition point will jump to the boundary layer at a sufficiently high Reynolds number. A sketch of transition distance in model diameters vs a pertinent Reynolds number based on body diameter is shown in Figure 2, based upon the above arguments. It appears from ballistic-range and wind-tunnel measurements using blunt bodies that in the intermediate Reynolds number region, $x/D \sim (Re\ D)^{-1}$ or $Re\ x = const.$[4] This implies that we may define a "transition Reynolds number" which is independent of body size. It must be borne in mind that such an artifice must be discarded when transition approaches the neck region. The effects of shape upon the transition Reynolds number is not clear, but marked differences between the values for spherical and conical models[5] indicates that a strong shape effect exists.

For the phenomenon of wake transition to be of practical use in reentry detection and discrimination, it is essential to relate transition to body or flight parameters. As stated previously, transition should be determined by the local wake conditions, and indeed good correlations of this type have been obtained[6] by basing Reynolds numbers on wake width and calculated wake edge conditions. In this way, body shape and flight conditions are accounted for but are not easily related to transition. Zelberg[5] has succeeded in correlating ballistic range data of others[5-7] accounting for body shape by modifying the transition Reynolds number as $Re_\infty x\left(\frac{M_\infty}{M_e}\right)^2$ where $Re_\infty x$ is based on free-stream conditions and M_∞ and M_e are the flight and wake edge Mach numbers. Once again, however, M_e is not easily related to the body shape.

For a given body shape, simple correlations are available. A Reynolds number based on free-stream conditions seems to be satisfactory for correlating x D at constant flight Mach number. In fact, even the product $p_\infty D$ appears to suffice.[7] If shape effects are to be correlated, however, it is necessary to have a better understanding of the transition mechanism and resort must be made to analyses of wake stability.

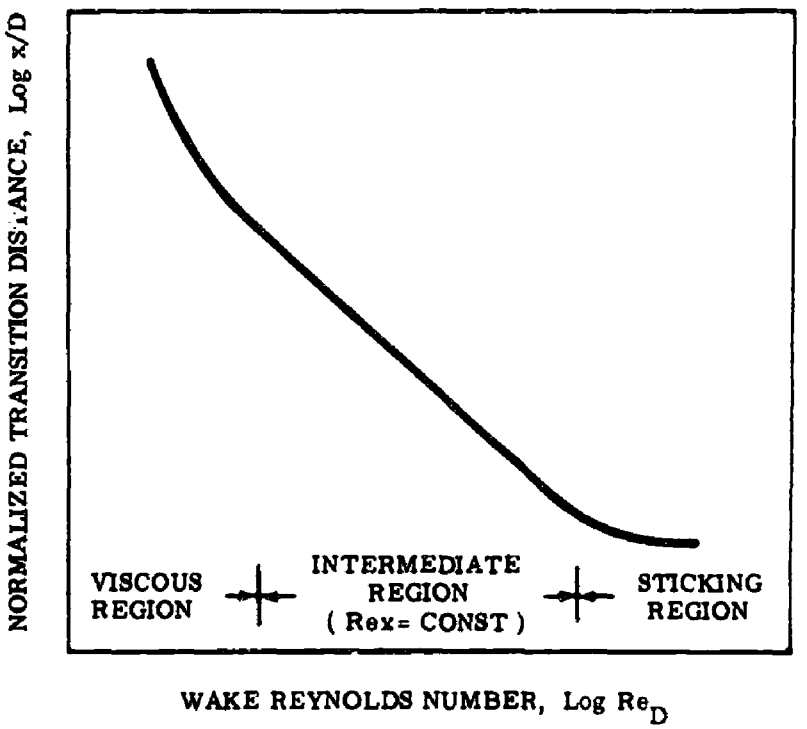

Figure 2 Variation of Transition Distance with Reynolds Number in Wakes

The linear region as defined in Reference 3 is the most amenable to analysis of the three regions. The initial amplification of sinusoidal oscillations can be treated by a linearized theory such as the Orr-Sommerfield approach. Most notable of the analyses of recent date which bring an insight into the hypersonic wake stability problem are the calculations of Sato and Kuriki[3] for two-dimensional incompressible wake flows; the work of Batchelor and Gill[9] for axisymmetric incompressible wake-type flows; and the extension of this work to compressible flows by Gold.[10] In all cases the effects of viscous dissipation are excluded (high Reynolds number assumption), and it is assumed that the flow is unstable only to subsonic disturbances.

In order that a disturbance be subsonic, the phase velocity of the disturbance relative to the surrounding fluid (c_R) must satisfy the condition

$$(c_R) < a_e \qquad \text{(Condition 1)}$$

where a_e is the sound speed in the fluid at the edge of the wake. Lees and Lin[11] have shown that a neutral subsonic disturbance must have a wave speed equal to the fluid velocity (w_c) at the point where the gradient of the density-vorticity product is zero, i.e.,

$$(c_R) = w_c \qquad \text{(Condition 2)}$$

where w_c is measured relative to the surrounding (wake edge) flow. Gold[10] has calculated w_c as a function of $\frac{\Delta T}{T_e} = \frac{T_o - T_e}{T_e}$ where T_o and T_e are the viscous wake centerline and wake-edge temperatures respectively. The results indicate a rapid decrease in c_R as $\frac{\Delta T}{T_e}$ is increased. Both conditions (1) and (2) must be met for a subsonic neutral disturbance to exist. In the case of a blunt body a_e is high but c_R is also high since $\frac{\Delta T}{T_e}$ is low (flow field shock-dominated). For a more slender body a_e is lower, but also c_R is lower since $\frac{\Delta T}{T_e}$ is higher (flow field boundary-layer dominated). Because of this, Lees[4] indicates that subsonic disturbances can exist (wake no longer Mach-number stabilized) fairly near the neck for both blunt and slender bodies. However, the amplification rate of the disturbances is also dependent upon $\frac{\Delta T}{T_e}$ and hence

upon the body slenderness. Gold[10] further shows that the amplification rate is higher for low $\frac{\Delta T}{T_e}$. In other words, even though subsonic disturbances can occur for slender bodies, they may require considerable distances to amplify before a transition point is observed.

From these considerations one might expect the blunt bodies to exhibit an early transition with rapid amplification and an accompanying short region to full turbulence. The very slender models, on the other hand, should exhibit a later transition and a long region for amplification, behaving much as the low-speed transition of Sato and Kuriki.

The slenderness of a body by these arguments has not been related entirely to its shape but rather to the temperature difference between the inviscid and viscous wakes. The outer wake temperature is controlled by the body shape but the inner viscous wake is affected not only by the shape but also by viscous effects on the body or by the viscous drag. On the other hand, the shock shape and hence inviscid wake heating is largely determined by the pressure drag of the body. This immediately suggests that the temperature difference $\frac{\Delta T}{T_e}$ is largely determined by the ratio $\frac{C_{Df}}{C_{Dp}}$ where C_{Df} is the friction (viscous) drag coefficient*, and C_{Dp} is the pressure (shock) drag. It appears then that C_{Df}/C_{Dp} should be a suitable shape parameter for correlating transition behind bodies of various axisymmetric shapes. This parameter has been used to correlate the results of the present investigation.

* To be more precise, the wake drag, C_{Dw} should be used. However, for cone-like bodies, $C_{Dw} \simeq C_{Df}$ since the drag due to the trailing shock is negligible. This is not the case for spheres, however.

III EXPERIMENTAL STUDIES

1. General Observations

The wake-transition studies were performed in the GM DRL Aerophysics Range, where launching techniques have been developed so that saboted conical models can be launched at speeds up to 24,000 fps. A series of cone models were launched with semi-vertex angles (θ) from 6.3 to 45 degrees and nose-to-base radius ratios (R_N/R_B) from .06 to 1. Spherical models of 2.5-, 5-, and 15-mm diameter were also used. The models were copper coated to delay ablation effect and ballasted where necessary to achieve a favorable margin of stability. A sketch of the models used and a list of model dimensions is given in Figure 3.

Transition distances were measured using an f/10 and an f/20 double-pass schlieren system, described in detail elsewhere.[12] The f/20 system employed a laser light source of 10-nanosecond exposure and the f/10 a spark source of 150-nanosecond duration, giving maximum model motion blurring of .003 and .040 inches respectively.

The schlieren system is sensitive to density gradients in the flow field. In the case of a blunt body where the temperature change $\frac{\Delta T}{T_e}$ is small, the density gradients are small and the viscous wake is barely discernible from the inviscid wake. The large density differences between the inviscid and viscous regions are clearly noticeable for the cone, however. A comparison between the schlieren photographs of the flow behind a sphere and a cone (see Figures 4, 7, and 9) points out this striking difference between shock-dominated and boundary-layer-dominated wakes.

The low contrast between the viscous and inviscid wake behind blunt bodies makes the transition point and the ensuing fluid motion very difficult to study from schlieren photographs. At low ambient densities and high flight Mach numbers, only the outer inviscid wake is observed (Figure 5). This inviscid trail extends behind the model for many hundreds of diameters. The physical

TR64-02K

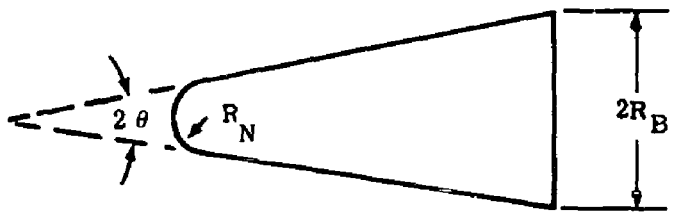

θ Degrees	R_B inches	R_N/R_B	M_∞	$Re_\infty D, M_\infty$	x, D	S (Eq. 2)
6.3	.125	.15	19.5	1.49×10^4	28	34
12.5	.125	.02	20.3	2.98×10^4	14	31
12.5	.125	.02	19.9	5.95×10^3	73	31
12.5	.125	.02	19.9	5.95×10^3	73	31
12.5	.125	.06	20.6	1.48×10^4	24	31
12.5	.125	.06	20.3	1.48×10^4	30	31
12.5	.125	.06	20.3	1.48×10^4	31	31
12.5	.125	.06	20.3	7.96×10^3	61	31
12.5	.125	.06	20.3	7.96×10^3	55	31
12.5	.125	.06	20.0	1.48×10^4	30	31
12.5	.125	.06	20.0	1.48×10^4	30	31
12.5	.125	.06	20.0	9.90×10^3	39	31
12.5	.25	.03	17.7	1.19×10^4	39	31
12.5	.125	.125	20.7	9.90×10^3	50	30
12.5	.125	.16	18.2	9.90×10^3	37	29
12.5	.125	.16	18.2	9.90×10^3	37	29
12.5	.188	.19	17.6	1.52×10^4	15	27
12.5	.188	.19	17.6	1.52×10^4	14	27
12.5	.125	.25	21.0	2.98×10^4	8	24
12.5	.125	.25	20.9	1.48×10^4	17	24
12.5	.125	.25	20.0	2.98×10^4	7	24
12.5	.125	.25	20.0	2.98×10^4	7	24
12.5	.125	.24	19.0	1.99×10^4	13	24
12.5	.125	.32	19.8	9.9×10^3	19	17
12.5	.188	.38	16.6	1.52×10^4	9	14
12.5	.188	.38	16.3	3.04×10^4	5	14
12.5	.125	.5	17.2	3.97×10^4	4	10
22.5	.25	.16	16.7	1.99×10^4	8	9.5
30	.25	.16	17.5	1.99×10^4	7.5	4.7
30	.25	.16	17.5	1.99×10^4	8	4.7
30	.25	.16	17.1	1.99×10^4	9	4.7
30	.25	.16	16.2	1.99×10^4	10	4.7
30	.25	.16	15.6	1.99×10^4	7	4.7
30	.25	.16	13.9	1.99×10^4	8	4.7
45	.25	.16	17.4	1.99×10^4	8	1.4
45	.25	.16	17.2	1.99×10^4	8	1.4

Figure 3 Model Shapes and Dimensions

size of the viscous wake within this trail can be estimated from the schlieren photograph of Figure 6 in which the wake was inadvertantly seeded with ablation products from a break in the model skin, making the viscous wake faintly visible. For smaller models, the outer wake becomes more pronounced (Figure 7) since the density gradients become much more severe.

The boundaries of the inviscid wake are very well marked in the flow behind cones (Figure 4) because of the large density gradient generated at the intersection of the conical body shock with the expansion wave from the base.

The inviscid wake diameter (b) increases at a rate independent of the model shape, depending only on the free-stream Reynolds number and the initial wake size (about one body diameter). A good correlation for the growth law of both spherical and conical models is, by reference to Figure 8,

$$b/D \sim \left(\frac{x/D}{Re_\infty D}\right)^{1/4}$$

This growth is somewhat slower than the growth of the turbulent wake at large distances behind the model, viz.,

$$(b/D)_{turb} \sim \left(\frac{x}{D}\right)^{1/3}$$

and may be much slower near the body, depending upon the body shape. It is of interest to note, at least for the case of a cone, that the laminar viscous wake grows slightly less rapidly than the outer wake. Hence, we may expect the inner wake to remain imbedded within the outer wake until some distance beyond transition. We expect, then, that turbulence behind blunt bodies at very low Reynolds numbers will not be observed by the use of schlieren techniques until the turbulence has grown through the surrounding hot fluid. Upon emergence of the turbulence through the inviscid core, strong Mach-type disturbances are generated in the surrounding flow when the local Mach number is sufficiently high.

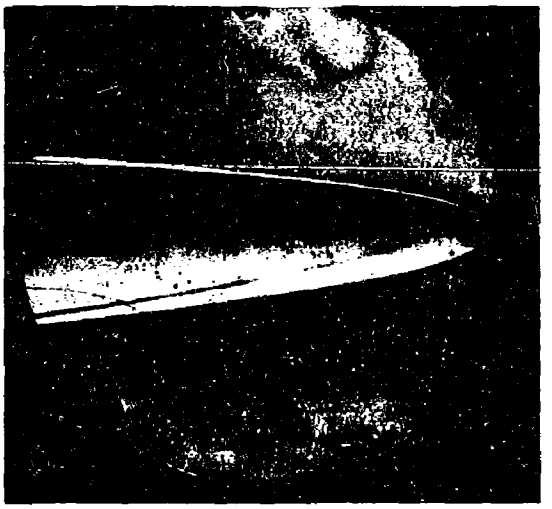

◄ a) SPHERE, M=19. p=30mm Hg, D=15mm

b) BLUNT CONE, M=17.5, p=50mm Hg, ► D=1/2 inch, $\Theta=30^{o}$, $R_N/R_B=.16$

◄ c) SLENDER CONE, M 20, p 75mm Hg, D-1 4 inch, Θ -12-1 2^{0}, R_N/R_B .02

Figure 4 Schlieren Photographs of Flow Behind Blunt and Slender Bodies

TR64-02K

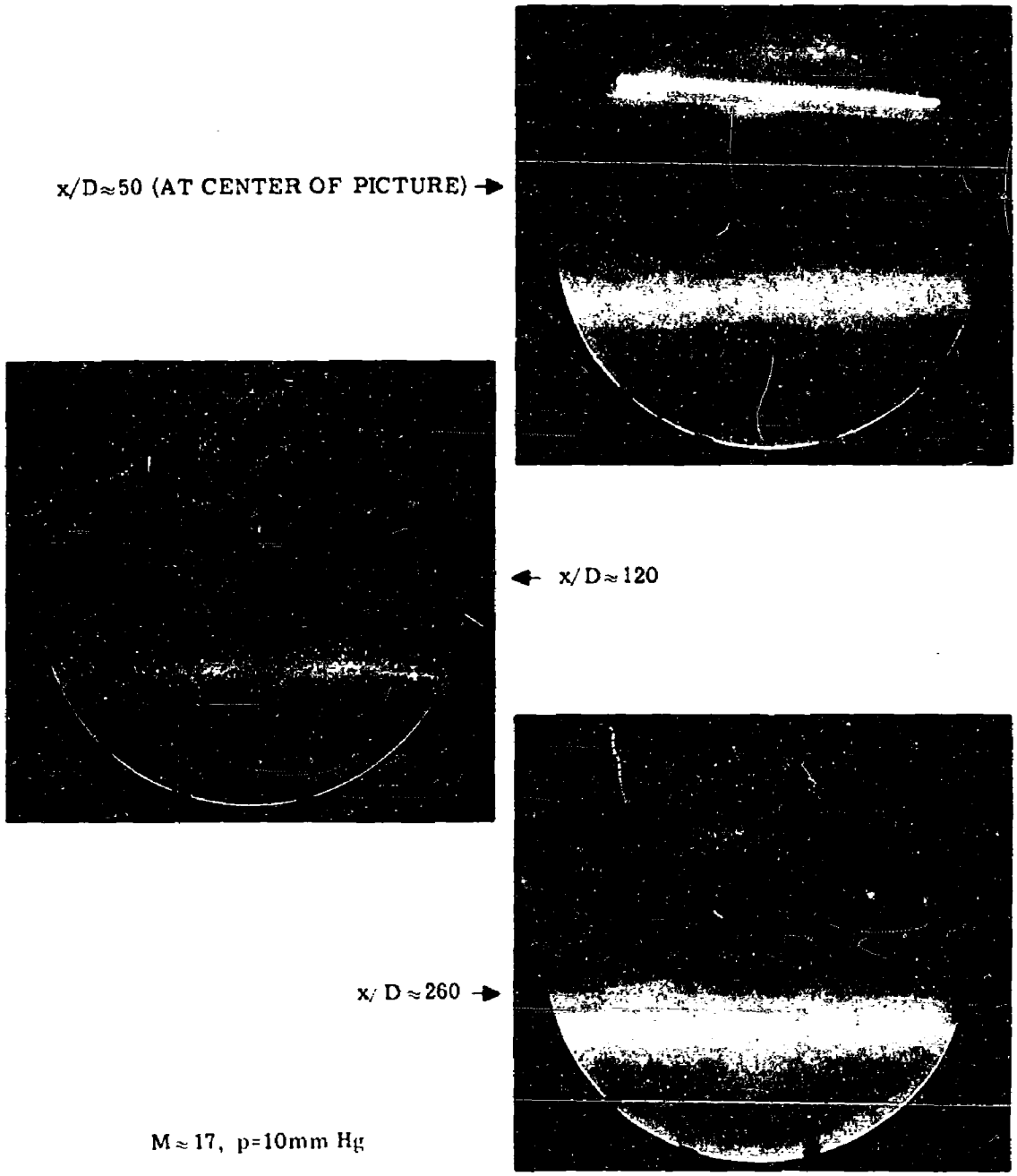

Figure 5 Inviscid Trail Behind a 15-mm-Diameter Sphere

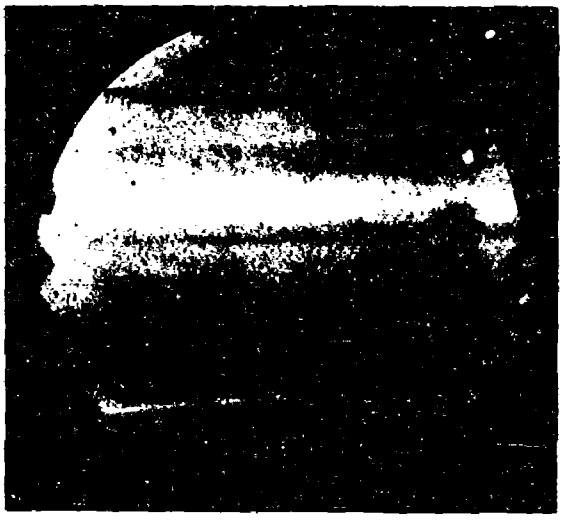

D=15mm
M=18
p=10mm Hg

Figure 6 Viscous Wake of Sphere Made Visible by Seeding with Ablation Products

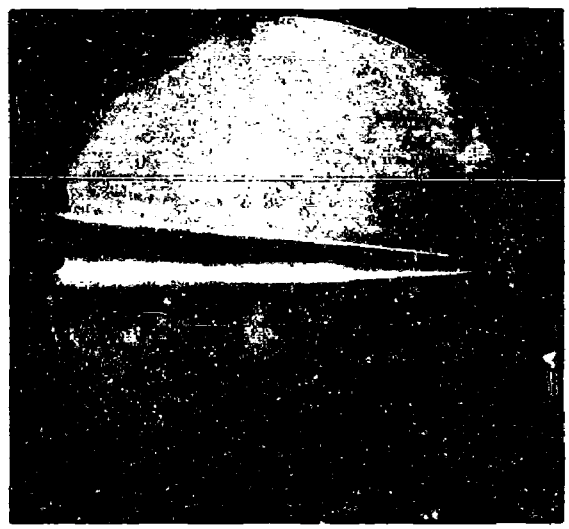

x/D≈50 (AT CENTER OF PICTURE)

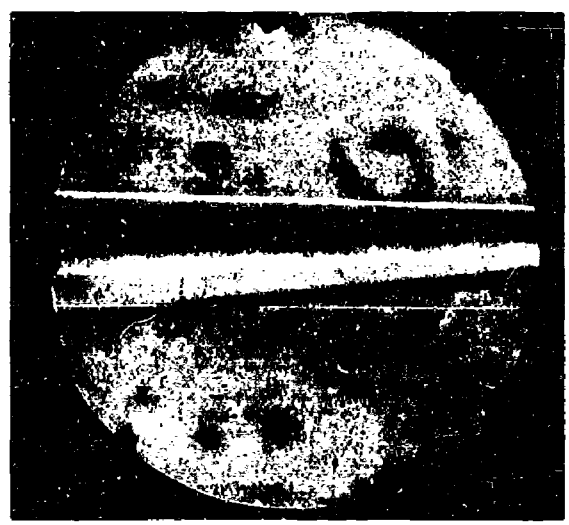

x/D = 120

M = 20, p = 18mm Hg

Figure 7 Inviscid Trail Behind a 2.5-mm-Diameter Sphere

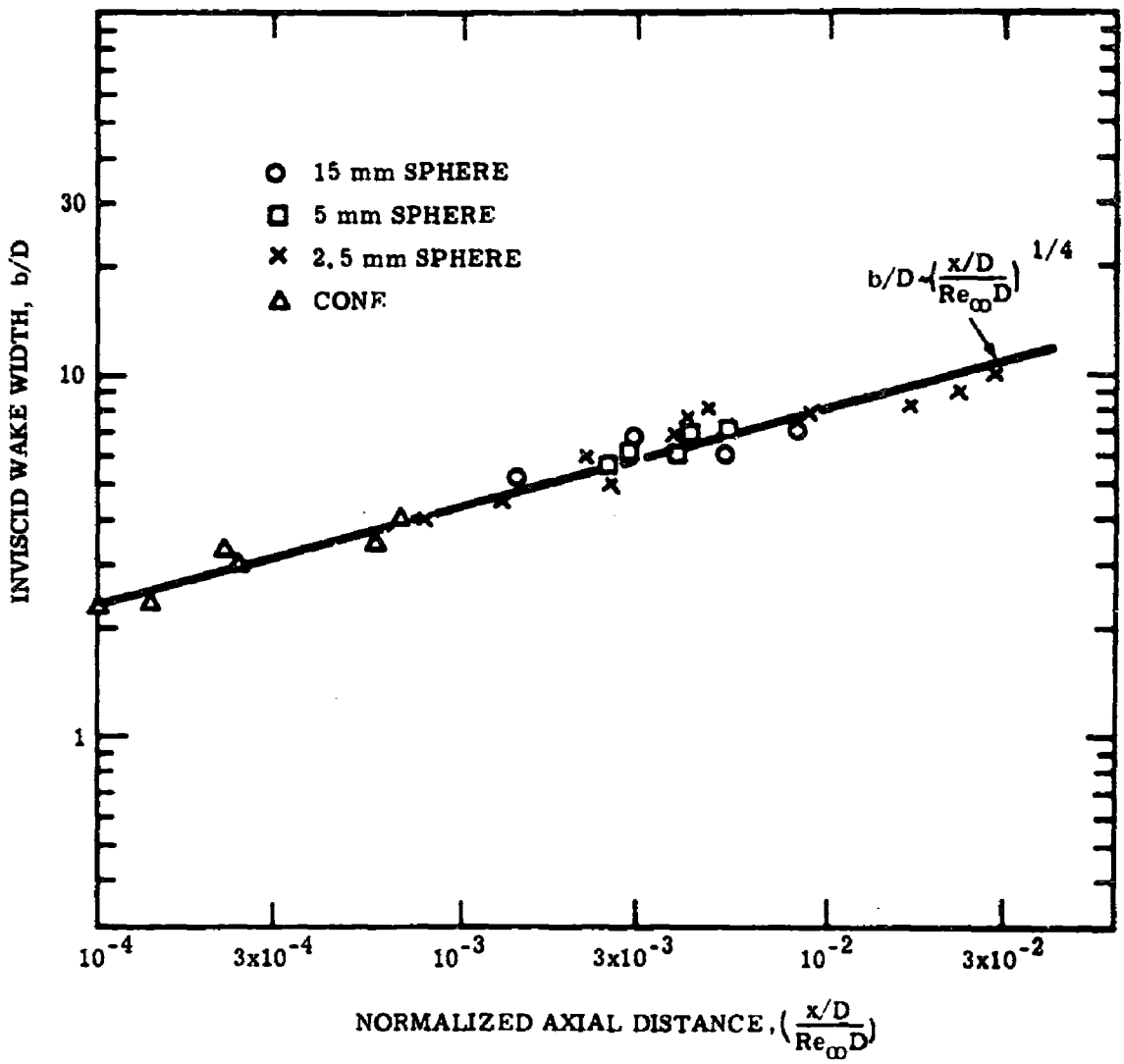

Figure 8 Growth of the Inviscid Wake

Striking differences in the mechanism of breakup of the laminar wake between blunt and slender bodies are evident from comparisons of the schlieren photographs of each (Figures 4, 9, and 10). For blunt bodies, transition in general occurs abruptly, changing from a straight laminar flow to what appears to be well developed turbulence within a few body diameters. On the other hand, for slender bodies, small oscillations are noticed in the viscous wake, in some cases requiring 50 to 100 diameters to amplify into large-scale periodic oscillations of the whole wake (Figure 9). These periodic oscillations then break up into large irregular patches of turbulence and finally form a somewhat homogeneous turbulent wake. This behavior is somewhat reminiscent of the behavior of transition behind flat plates as observed by Sato and Kuriki, viz., a linear region amplifying to form a nonlinear region and finally, a three-dimensional distortion before forming fully developed turbulence.

The general behavior of the blunt- and slender-body transitions is therefore in general agreement with the earlier discussions. For blunt bodies, amplification rates are rapid and transition occurs rapidly once subsonic disturbances are allowed. For slender bodies amplification rates are slow and the complete transition process is a long, gradual one.

The mechanism of transition is strongly influenced by ablation products in the wake. Particularly, at high ambient pressures ablation can modify the flow field as recorded on schlieren photographs.

The effect of ablation may be seen from Figure 10, which gives a comparison of a nonablating cone, a slightly ablating cone (from sharp edges on the base), and a cone whose flow is deliberately seeded with an epoxy from an ablation ring on the cone surface. The relative amount of ablation (or its absence) was determined by image-converter photographs of the radiation from the model, and from the level of electron and radiation observables. It may be seen that the transition behind the nonablating cone occurs well behind the model, with a long smooth laminar region. With slight ablation effects, transition occurs much earlier but still with a relatively long transition process. With heavy

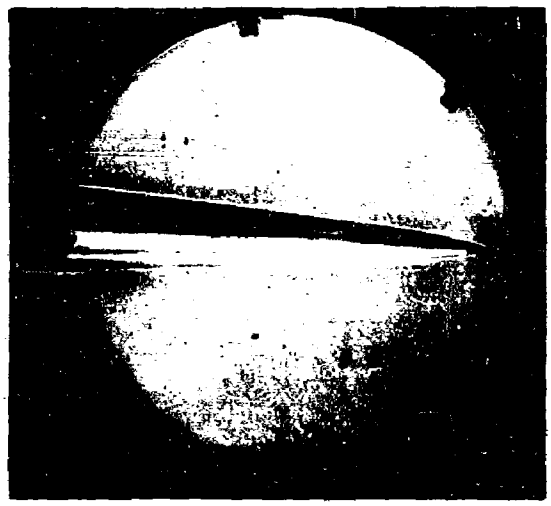

← NO ABLATION

MODERATE ABLATION →

← HEAVY ABLATION

M_∞ -20, p_∞ -75mm Hg

Figure 9 Effect of Ablation on Wake

TR64-02K

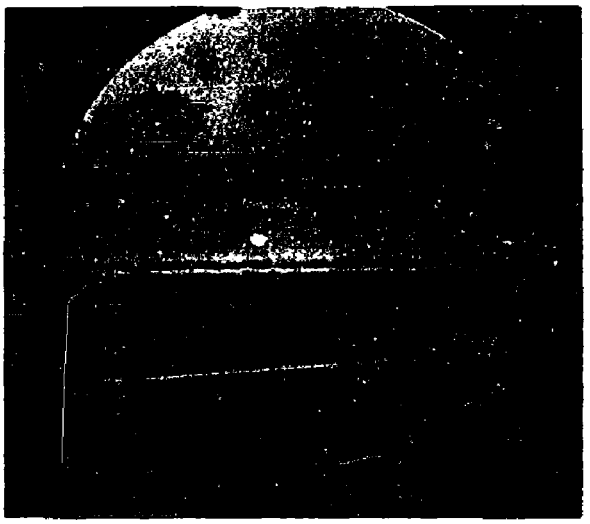

a) x/D≈80 (AT CENTER OF PICTURE)

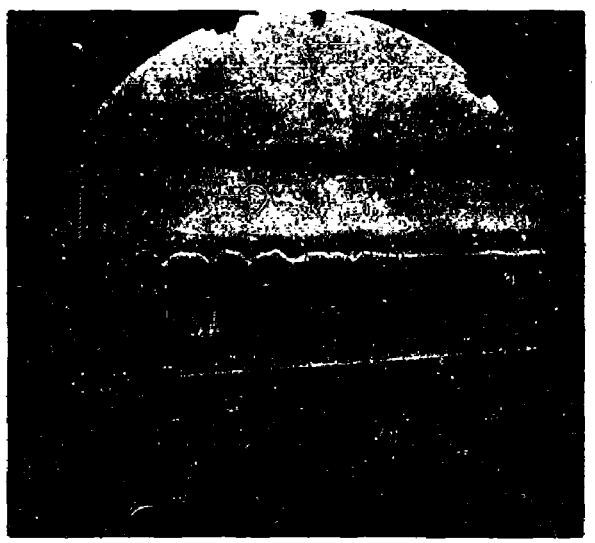

b) x/D≈140

$\theta = 12 \cdot 1/2^{\circ}$, $R_N R_B$ .02, p=30mm Hg, M=20, D-. 25 inch

Figure 10 Transition in the Far Wake of a Slender Cone

ablation, however, transition occurs very close to the base of the cone and full turbulence develops rapidly.

Ablation effects appear to be minimal at ambient pressures of 50 mm Hg and below. At 75 mm Hg light ablation could result in a total scatter of the present transition results up to 50% depending upon nose bluntness and flight speed. In light of this, results obtained using sharp cones at pressures above 75 mm Hg must be accepted only with the utmost caution.

2. Transition Correlations

In agreement with the earlier definition of a transition point, transition distances were measured on schlieren photographs from the model nose to the first appearance of disturbances in the viscous wake. Any other definition would be difficult to assess since the boundaries of the various regions of transition, in the case of slender bodies at least, are ill-defined. Further, of course, any recourse to, or comparison with, existing transition theories must be made under conditions where linear theories are applicable.

It was early determined that the location of transition was strongly dependent upon angle of attack of the conical models. For this reason, only those rounds were used for data analysis which had an angle of attack less than one-half the semivertex angle of the cone throughout the complete flight of the model. Further, because of the strong influence of ablation products, only those rounds were analyzed where it was indicated that no ablation was present. These rounds are tabulated in Figure 3. Because of essential differences between the cone and sphere transition results, the two types of models will be discussed separately.

A. Spheres

The normalized transition distance x_t/D for spheres could be correlated by the free-stream Reynolds number $Re_\infty D = \frac{\rho_\infty V_\infty D}{\mu_\infty}$ (Figure 11) for the

TR64-02K

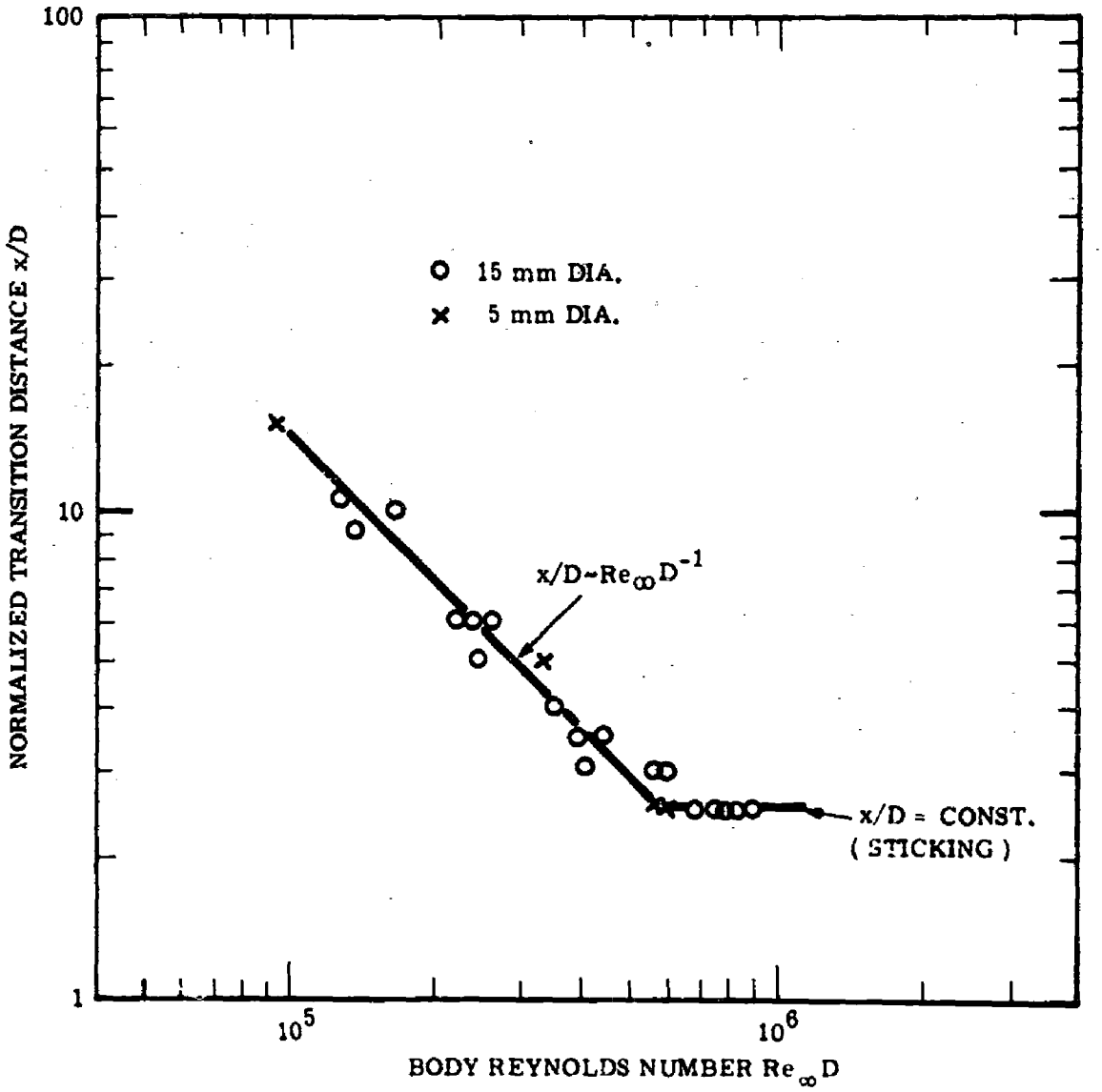

Figure 11 Transition Data for Spheres ($14 \cdot M_{(t)} \cdot 20$)

relatively small spread of flight speeds ($15 < M < 19$). The shape of the plot of x/D vs $Re_\infty D$ is in good agreement with the sketch of Figure 2, at high Reynolds numbers. No data was obtained at low Reynolds number because the laminar wake presented insufficient contrast on the schlieren photographs to be discernible, as explained previously. For the 15-mm-diameter sphere, the lowest ambient pressure for which data was obtained was 17 mm Hg. For the smaller spheres, the limit was correspondingly higher.

In the intermediate Reynolds number range, $x/D \sim Re_\infty D^{.1}$ or $Re_\infty x$ = constant $\simeq 1.4 \times 10^6$ for all spheres (Figure 11). At higher Reynolds number, transition "sticks" in the neck and x/D = const. Transition point "sticking" occurs at a Reynolds number independent of body size for the small range of sphere diameters studied. In general, we would expect a dependency on both Mach number and Reynolds number, since both these parameters affect the location of the neck. The dependency will be much stronger for cone shapes than for spheres because of the effect of the thicker boundary layers of conical models upon the base flow.

The transition distance behind spherical shapes appears to be relatively insensitive to flight speed, a fact also noticed by others.[7, 13] As a result, it was found that the effect of Mach number on transition could be accounted for at the high Mach numbers by using a transition Reynolds number $\frac{Re_\infty x}{M_\infty} = \frac{\rho_\infty a_\infty x}{\mu_\infty}$ A plot of $\frac{Re_\infty x}{M_\infty}$ vs M_∞ is shown in Figure 12, for values of $Re_\infty D$ where "sticking" does not occur. Also included in the plot are the early results of Slattery and Clay;[7] only the "scatter bars" are shown for the latter. It is seen that the speed-independent transition Reynolds number is only slightly dependent on Mach number at low Mach numbers, and appears to become constant at high Mach numbers, giving

$$Re_\infty x \simeq 8 \times 10^5 M_\infty \quad \text{for } M_\infty > 10 \qquad (1)$$

TR64-02K

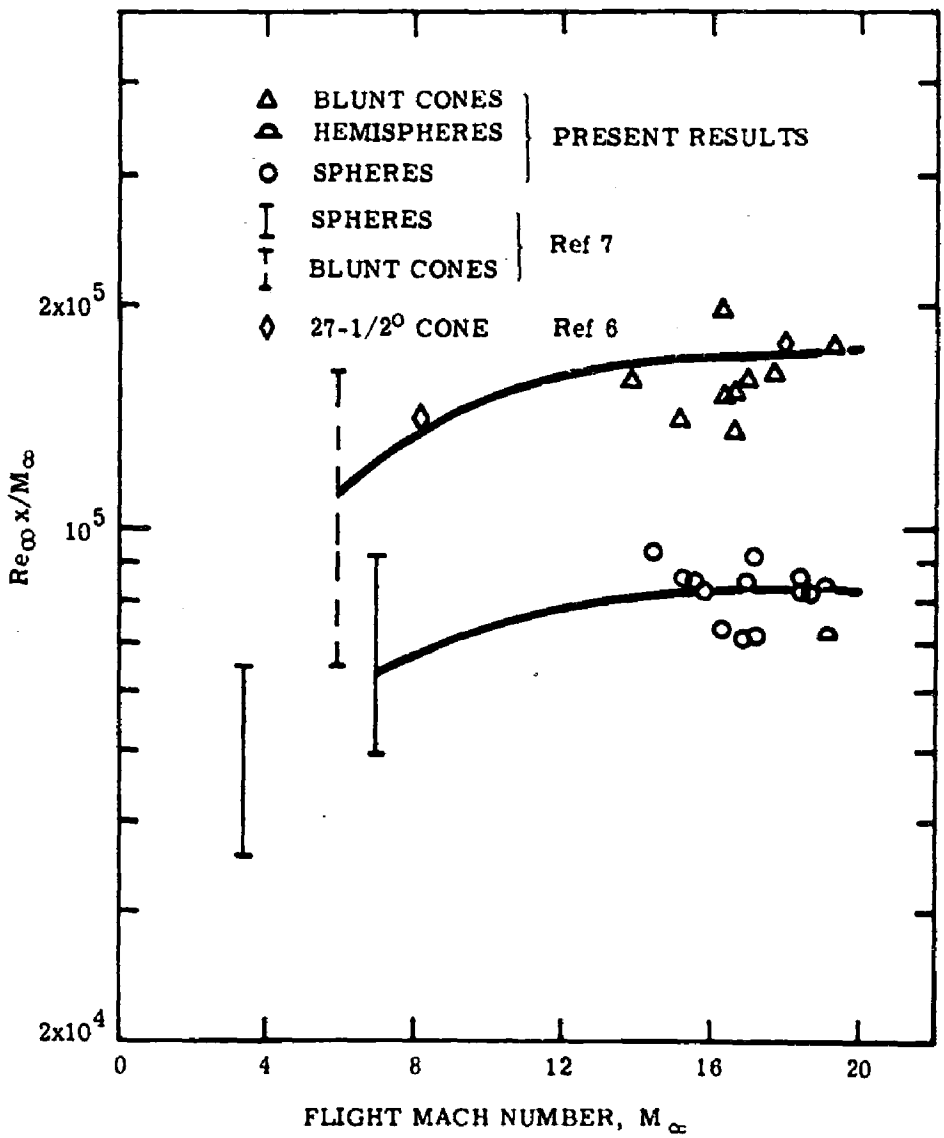

Figure 12 Effect of Flight Mach Number on Transition Reynolds Number for Spheres, Hemispheres, and Blunt Cones

More recent results of Slattery and Clay[14] show much higher values of $Re_\infty x$, particularly at low ambient pressures. There is some possibility, however, that these results were actually a measure of the position at which the turbulent wake emerges from the surrounding inviscid layer, rather than a measure of transition distance.[14]

B. Cones

In attempting to correlate the transition data of the cone and blunt-cone wakes, it became apparent that the transition distances at Mach numbers above 14 were insensitive to flight speed and a modified transition Reynolds number $\frac{Re_\infty x}{M_\infty}$ could be obtained for each body shape; further, its value was independent of body shape for the blunt bodies and was about a factor of 2 higher than the value for spheres.

The values obtained for $\frac{Re_\infty x}{M_\infty}$ for a variety of blunt shapes are shown in Figure 12 as a function of M_∞, along with results of Slattery and Clay at low M_∞. The same trend with Mach number is noticed for the blunt cones as for spheres, with a high Mach number-transition Reynolds number of

$$Re_\infty x = 1.6 \times 10^5 M_\infty \qquad (2)$$

The sphere cannot be considered geometrically similar to the blunt cone, i.e., a cone with $R_N/R_B = 1$, since the base shapes are different. In order to determine if this difference was responsible for the higher $Re_\infty x$ for blunt cones, hemispherical models were launched and the results are also plotted in Figure 12. It can be seen that there is no difference between the transition behind these models and behind spheres within the experimental scatter. A possible reason for the difference is the small contribution of the boundary layer to the initial wake drag for spheres and hemispheres, the trailing shock[15] producing essentially all the drag in the wake. This would have an effect on the wake-temperature profile and, consequently, on the phase velocity of neutral distrubances c_R.

In an attempt to correlate the transition Reynolds numbers for the slender bodies, resort was made to the slenderness parameter C_{Df}/C_{Dp} discussed earlier. In order to accomplish this, a knowledge of the pressure drag coefficient C_{Dp} and the friction drag coefficient C_{Df} are required. The graphs given by Lees and Hromas[15] were used to estimate C_{Dp} and are reprinted in Figure 13. The friction drag was calculated from flat plate, laminar boundary layer considerations applying the compressibility corrections given by Van Driest[16] and assuming all models were pure cones (no blunting) after the fashion of Reference 15. The boundary-layer edge conditions were determined using the cone calculations of Romig.[17] It was found that C_{Df} was independent of speed in the range $10 < M_\infty < 20$ to within ± 5% when correlated with respect to free-stream conditions. Thus, the calculated curve of $C_{Df}\sqrt{\frac{R_\infty D}{M_\infty}}$ vs θ given in Figure 14, was used in the determination of C_{Df}.

In Figure 15 a graph of the normalized transition distance x/D is plotted against C_{Df}/C_{Dp} on a logarithmic plot. It can be seen that to a good approximation $x/D \sim \left(\frac{C_{Df}}{C_{Dp}}\right)^n$ where n is approximately 2. Thus the transition distance can be correlated for slender body shapes by the relation

$$\frac{x}{D} = 400\left(\frac{C_{Df}}{C_{Dp}}\right)^2 \qquad (3)$$

The boundary between blunt-body (Equation 2) and slender-body (Equation 3) correlations can be determined from the plot of

$$\frac{Re_\infty x}{M_\infty} \text{ vs } \left(\frac{C_{Df}}{C_{Dp}}\right)^2 \frac{Re\, D}{M_\infty} \text{ given by Figure 16.}$$

The two lines representing Equations (2) and (3) intersect at

$$\frac{C_{Df}}{C_{Dp}}\sqrt{\frac{Re_\infty D}{M_\infty}} \simeq 20 \qquad (4)$$

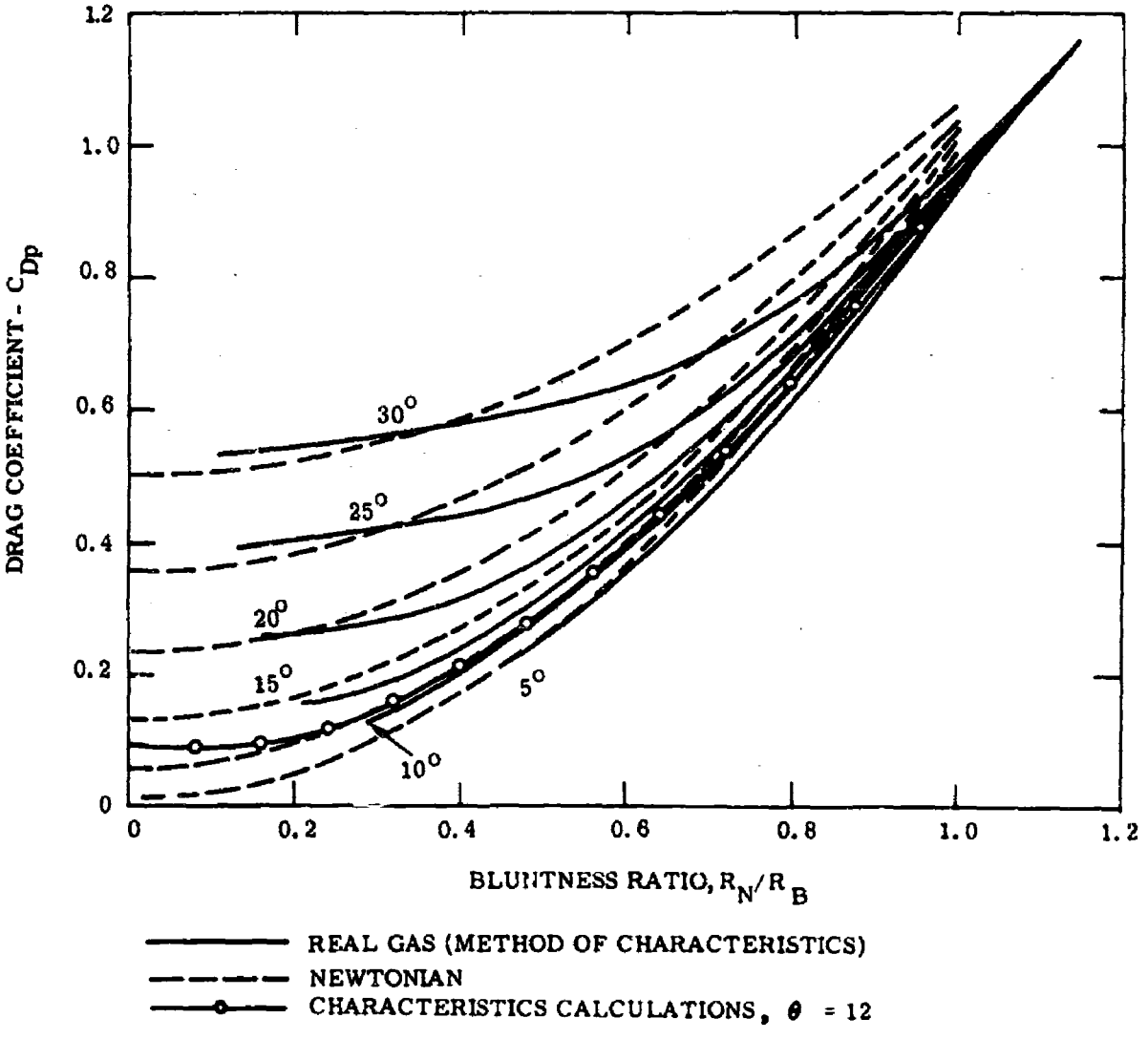

Figure 13 Pressure Drag Coefficient for Blunted Cones
(Reproduced from Reference 15)

TR64-02K

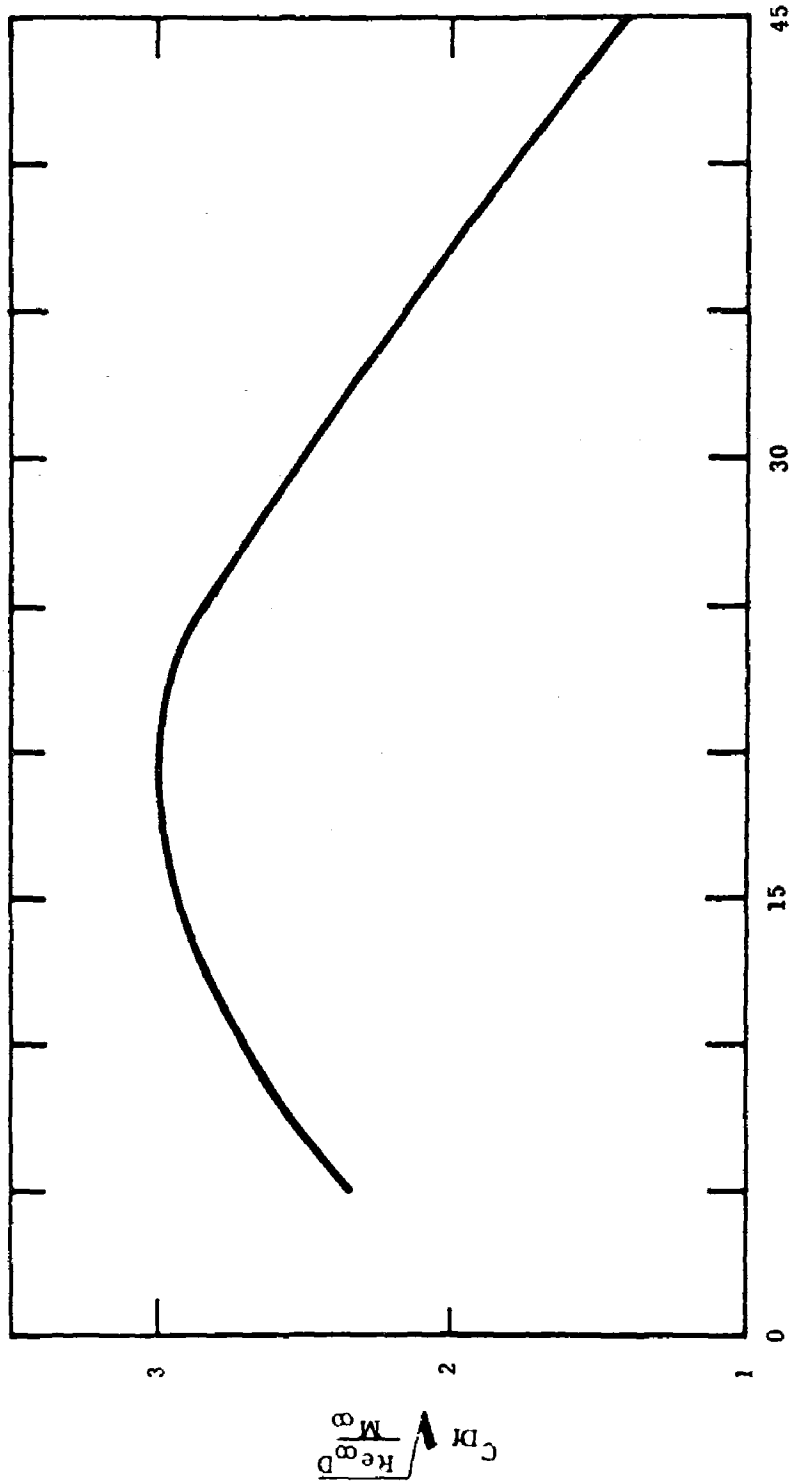

Figure 14 Friction Drag Coefficient for Cones ($M_\infty > 10$)

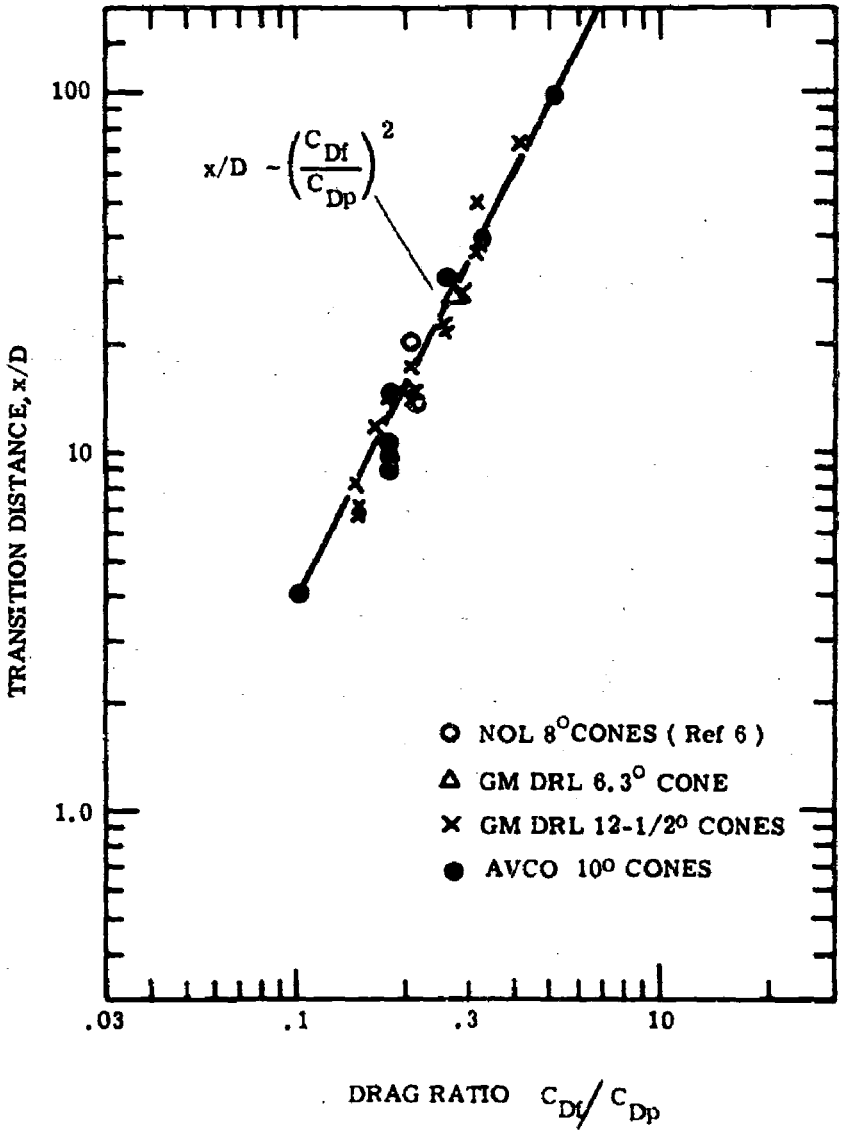

Figure 15 Transition Correlation for Slender Blunted-Cone Models

TR64-02K

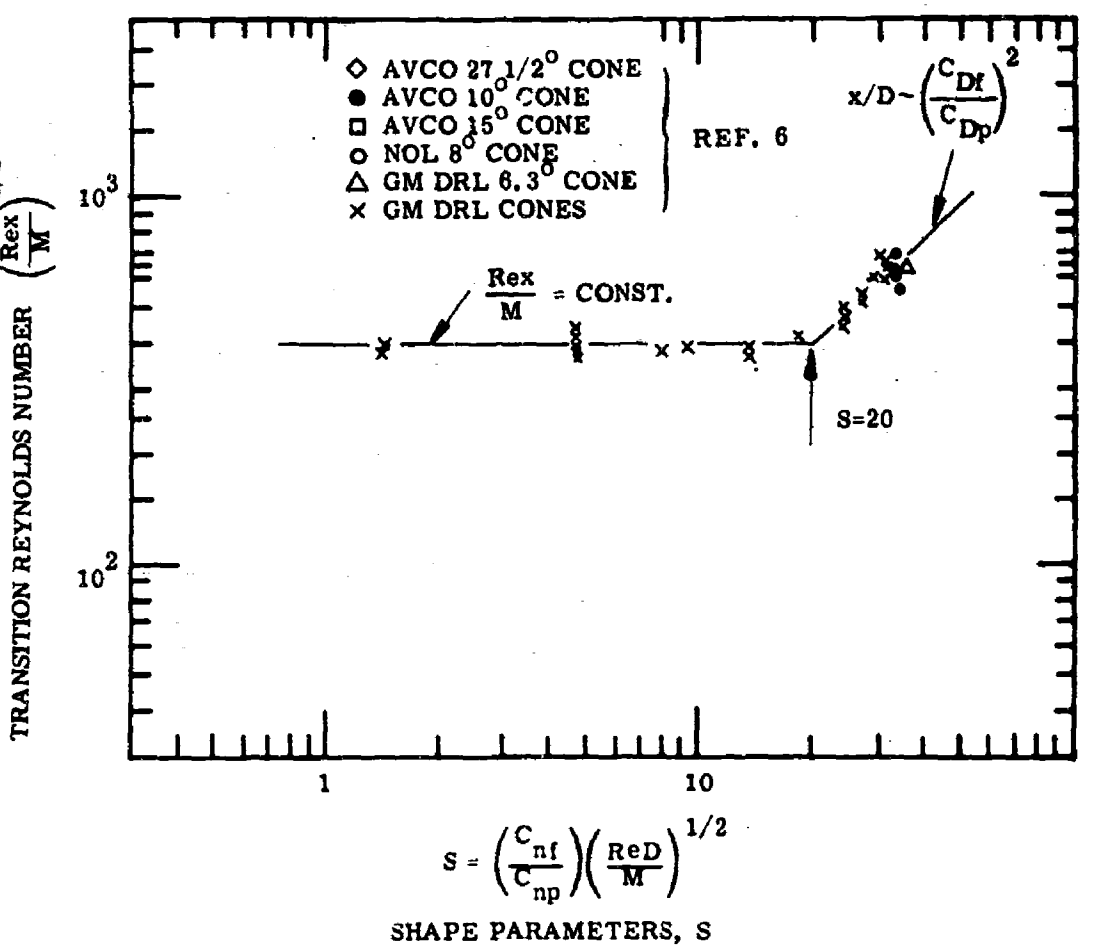

Figure 16 Blunt- and Slender-Body Correlations

The value of the shape parameter $S = \frac{C_{Df}}{C_{Dp}}\sqrt{\frac{Re_\infty D}{M_\infty}}$ then, indicates whether the body is slender so that Equation (3) applies, or blunt, in which case Equation (2) applies. Since $C_{Df}\sqrt{\frac{Re_\infty D}{M_\infty}}$ and C_{Dp} depend only on shape for axisymmetric bodies, S is a geometrical shape parameter only, being independent of ambient conditions, size, and speed.

The correlation of Equation (3), given by Figure 15 was made for a rather narrow range of flight Mach numbers. The effect of Mach number can be seen from Figure 17 in which the results of Reference 6 which satisfy the condition $S > 20$ are also plotted. At low speeds, some Mach-number effects are noticeable, but for $M_\infty > 10$ the correlation $\frac{x}{D}\sqrt{\frac{C_{Dp}}{C_{Df}}}$ = const. appears to hold very well. It may be noted here that since C_{Df} and C_{Dp} are velocity-independent for $M_\infty > 10$, the transition distances are also velocity-independent in the case of blunt bodies.

A further comparison of the present results with those of other investigators may be seen from Figure 16, which shows good agreement except perhaps for the 15-degree-cone results, which lie very near the boundary between slender and blunt shapes. These cones exhibit a higher transition distance than would be predicted by either Equation (2) or Equation (3). The differences are particularly noticeable at lower Mach numbers. One might conjecture that this shape of cone lies in a "transition" region between the two correlations.

Since $C_{Df}\sqrt{\frac{Re_\infty D}{M_\infty}}$ is dependent only on cone semivertex angle for nearly pointed cones, the correlation expressed in Equation (3) may be written $\frac{x}{D} \sim \frac{M_\infty}{Re_\infty D}$ for a constant shape or $Re_\infty x$ = const. M_∞ as was the case for blunt bodies. Hence, a transition Reynolds number may be defined for each axisymmetric body shape, independent of body size, in the intermediate Reynolds number range.

TR64-02K

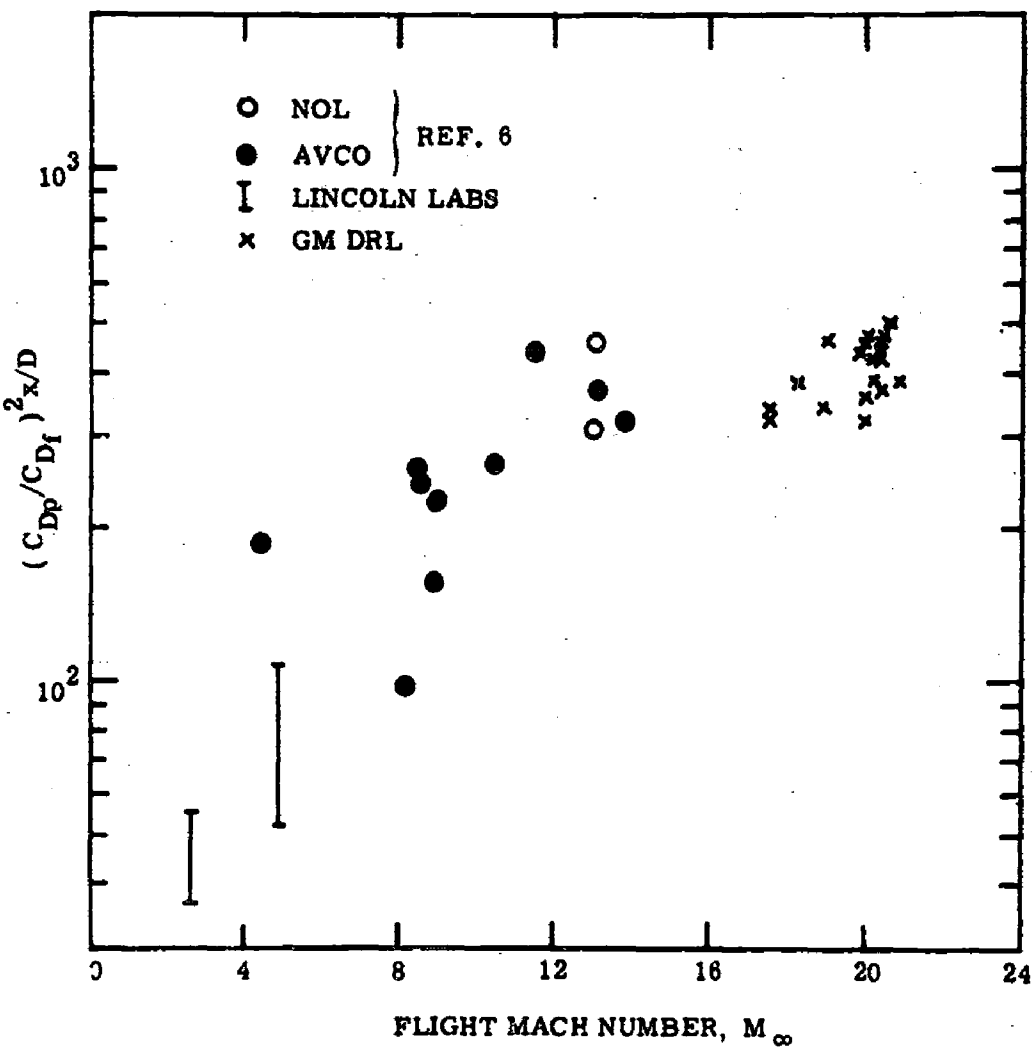

Figure 17 Effect of Flight Mach Number on Transition Behind Slender Bodies

The particular body shapes which satisfy the condition set by Equation 4 may be determined from Figure 18. In order for the slender-body correlation to apply, the bluntness ratio R_N/R_B must be less than 1.3 and the maximum semivertex angle must be less than 16°.

For cone angles below 16°, it is probable that the neglect of bluntness does not cause appreciable errors in the calculation of C_{Df}. As the angle decreases, the friction drag will reverse its trend and begin to increase. As a result we would expect the boundary curve of Figure 15 to behave somewhat as indicated by the dashed line in that figure.

Although no size-dependence of transition is allowed by the present correlation, it must be recalled that both the high-Reynolds-number (sticking effect)* and low-Reynolds-number (viscous effect) limits will be size dependent. Hence, the limits of $Re_\infty D$ over which this correlation is valid are yet to be determined. With this in mind, it is possible to use the results to predict the transition distance in clean wakes (no ablation) behind reentry vehicles.

To this end, Equation (3) may be written

$$x = \frac{400\,S^2}{\rho \frac{a}{\mu}}$$

Now $\frac{a}{\mu} \sim 3 \times 10^9$ ft^2/slug

Thus x (in feet) $= 5.60 \times 10^{-5} \frac{S^2}{\Gamma}$ (5)

where $\Gamma = \frac{\rho}{\rho_o}$ and ρ_o is standard atmospheric density.

---

* It is of interest to observe here that the phenomenon of "sticking" was not observed for the slender cones. At ambient pressures up to 150 mm Hg the transition point moved continually toward the body according to the correlation Equation (3).

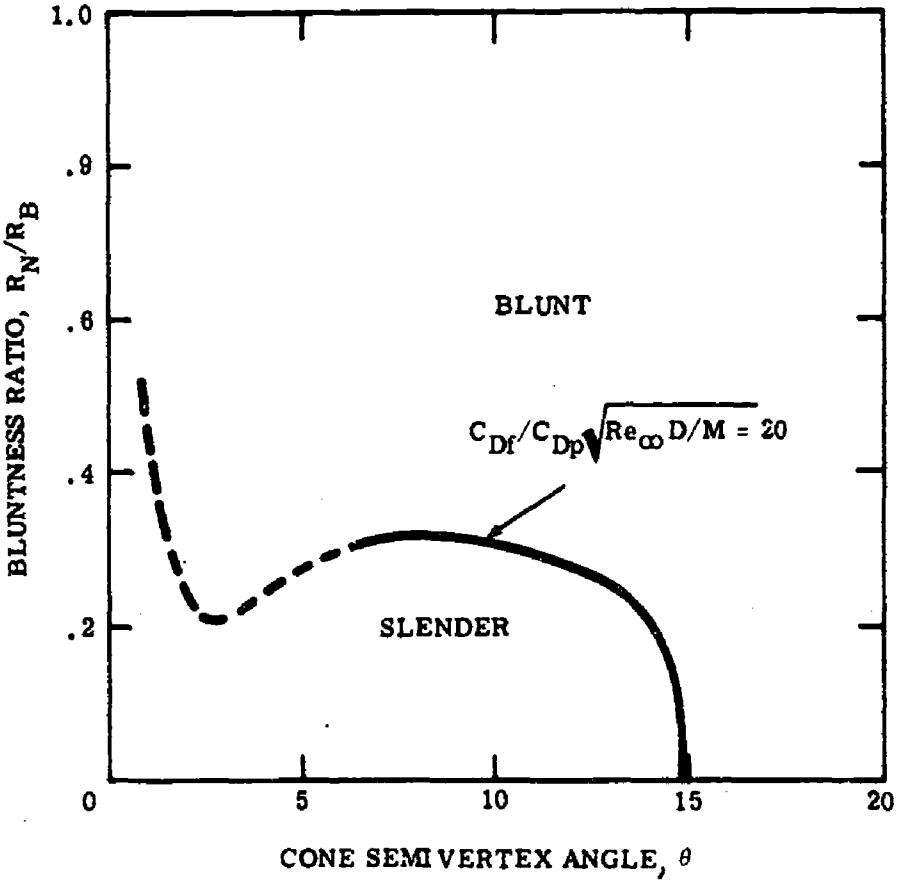

Figure 18 Slender- and Blunt-Body Regions

Equation (5) is plotted in Figure 19, which gives transition distance x in feet as a function of altitude and range pressure for various values of S. The variation of density with altitude has been assumed to be an exponential one. The shape parameter S for the particular body of interest may be determined from Figure 20.

Also plotted in Figure 19 are the correlations for spheres (Equation (1)) and for blunt cones (Equation (2)). If a measurement of x is made for an incoming reentry vehicle and the altitude is known, then the shape parameter S can be determined. This will then classify the body as spherical, blunt, or slender. If slender, the actual slenderness is known. Thus, these correlations offer a possible discrimination technique based on a measurement of transition distance. It must be stressed once again that the range of body Reynolds number ($Re_\infty D$) for which this correlation is valid has not been determined.

IV SUMMARY AND DISCUSSION OF RESULTS

The primary differences in the flow fields behind blunt and slender sphere-cone models can be traced to the relative importance between the inviscid and viscous regions of the wake, that is, to the extent to which the flow field is boundary-layer-dominated (slender body) or shock-dominated (blunt bodies.) It is this difference which determines whether the trail observables will be governed by the inviscid outer wake or by the viscous inner core. Further, it is this difference which governs in a strong fashion not only the growth of instabilities in the viscous wake, but also the extent and importance of Mach number stabilization of the wake.

It was this difference which pointed up the use of the ratio of the drag in the boundary layer to the drag associated with the shock, $\left(\frac{C_{Df}}{C_{Dp}}\right)$ as a parameter indicative of the relative importance of the bow shock wave and thereby a parameter through which body shape effects might be correlated.

TR64-02K

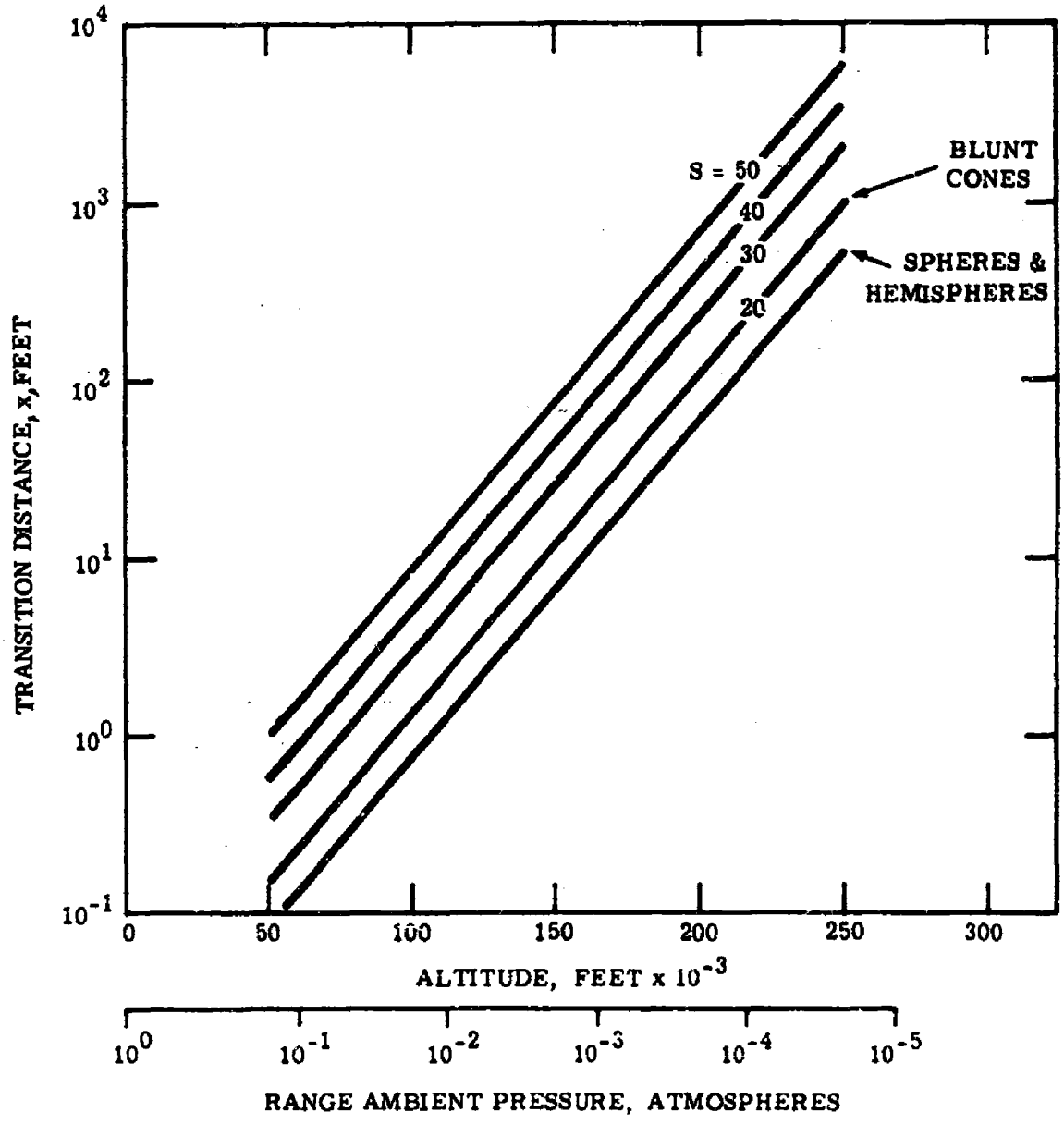

Figure 19 Predicted Transition Distances for Hypersonic, Axisymmetric Reentry Bodies

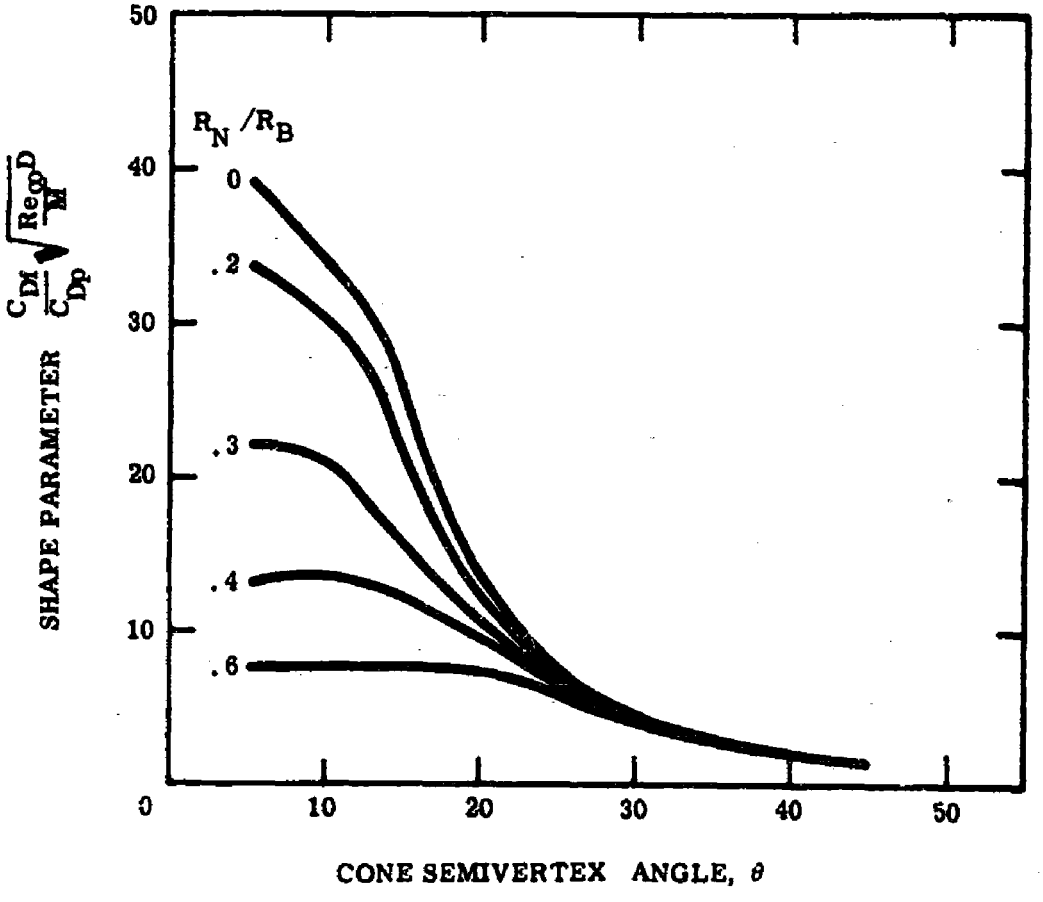

Figure 20 Shape Parameter for Blunted Cones

It was found that the primary shape parameter which described the shape of a body for purposes of correlating transition distances was $S = \frac{C_{Df}}{C_{Dp}}\sqrt{\frac{Re_\infty D}{M_\infty}}$, a function only of cone angle and bluntness ratio. For $S < 20$ the body behaved as a blunt body with a transition Reynolds number $Re_\infty x \simeq 1.60 \times 10^5 M_\infty$ typifying all blunted cone shapes and another $Re_\infty x = 8 \times 10^4 M_\infty$ typifying spherical and hemispherical shapes. The difference between these two values of Re x has been tentatively attributed to the importance of the drag introduced into the wake by the trailing shock in the case of a spherical model. For $S > 20$ a common transition Reynolds number does not exist for all shapes, but rather,

$$Re_\infty x \simeq 400\ S^2\ M_\infty \quad \text{or} \quad \frac{x}{D} \simeq 400\left(\frac{C_{Df}}{C_{Dp}}\right)^2$$

In all cases, the transition distances were independent of both body size and flight speed for Mach numbers above 10, except at very high body Reynolds numbers ($Re_\infty D$). At large $Re_\infty D$, the transition "sticks" in the neck region and the Reynolds number at which this occurs depends upon the body size, it is believed.

It appears then that bodies can be conveniently classified as blunt or slender, for our purposes, depending upon their value of $S = \frac{C_{Df}}{C_{Dp}}\sqrt{\frac{Re_\infty D}{M_\infty}}$. Further, it appears that the character of the transition process is radically different between the blunt and slender bodies defined in this way. For blunt bodies the transition to full turbulence appears to be abrupt, occurring within a few body diameters. For slender bodies the transition process occurs in several stages: small oscillations, large oscillations of the complete wake, irregular patches of turbulence and finally full turbulence, the whole process taking, in some cases, hundreds of diameters to complete. A tentative explanation for this behavior might be that in the case of the blunt bodies, amplification rates are so high as a result of the shock-dominated flow field that transition occurs abruptly once subsonic disturbances can exist. Where the flow field is boundary-layer dominated, however, the amplification rates would be low and the transition process would be longer for slender bodies.

At sufficiently low Reynolds numbers, we would expect these arguments and correlations to become invalid. Viscous dissipation then begins to play a dominant role, limiting the minimum Reynolds number at which transition can occur.

Because of the importance of the inviscid wake in the determination of the wake observables, some measurements were made of its growth. It was found that its growth rate was slightly more rapid than the viscous wake growth, and substantially less than the turbulent wake growth. Thus, turbulence eventually emerges from the inviscid region into the low-temperature surroundings. In the case of very blunt bodies the viscous wake could not be distinguished within the outer wake at low ambient pressure, since the schlieren system is insensitive to the small density changes occurring in the wake region of shock-dominated flow.

Keeping in mind the limitations and the dangers in extrapolating range results to full-scale observations, we can plot the transition distance behind axisymmetric bodies as a function of altitude. Using such a chart, the transition distance in clean wakes (no ablation effects) measured by down-range radar systems would give a direct indication of whether a body is blunt or slender, and if slender, a measure of its slenderness. The increase in transition distance from a blunt body to a slender cone shape is roughly a factor of 4 to 8, which should be discernible.

The effect of ablation in these results is not known. Where ablation is heavy, range experiments show that the whole transition process is masked by the ablation products. Even so, at higher altitudes before ablation becomes appreciable, a correlation such as given here may prove a valuable aid to discrimination techniques. A further factor, unsolved at the present time, involves the relationship between the radar backscatter from transition and the fluid-mechanical transition measured by a schlieren system. The coupling between the two is very complex and is the subject of a research study at GM Defense Research Laboratories at the present time under this same contract.

REFERENCES

1. Primich, R., and Steinberg, M., "A Broad Survey of Free-Flight Measurements of the Flow About Spheres and Cones," AMRAC Proceedings, Vol. IX, Oct 1963

2. Primich, R., et al, "Radar Scattering from Wakes," AIAA Bulletin, Vol. 1, No. 8, 1964

3. Sato, H., and Kuriki, K., "Transition in the Wake of a Thin Flat Plate Placed Parallel to a Uniform Flow," Jour. Fluid Mech., Vol. 11, Pt. 3, Nov 1961

4. Lees, L., "Hypersonic Wakes and Trails," AIAA Journal, Vol. 2, No. 3, Mar 1964

5. Zelberg, S.L., "Transition Correlations for Hypersonic Wakes," AIAA Journal, Vol. 2, No. 3, Mar 1964

6. Pallone, A., Erdos, J., and Eckerman, J., "Hypersonic Laminar Wakes and Transition Studies," AIAA Journal, Vol. 2, No. 5, May 1964

7. Slattery, R.E. and Clay, W.G., "The Turbulent Wake of Hypersonic Bodies," ARS Preprint 2673-62, Nov 1962

8. Slattery, R.E. and Clay, W.G., "Laminar-Turbulent Transition and Subsequent Motion Behind Hypervelocity Spheres," ARS Journal, Vol. 32, 1962

9. Batchelor, G.K. and Gill, A.E., "Analysis of the Stability of Axisymmetric Jets," Journal Fluid Mech., Vol. 14, Pt. 4, Dec 1962

10. Gold, H., "Stability of Laminar Wakes," PhD Thesis, CIT, 1963

11. Lees, L. and Lin, C.C., "Investigation of the Stability of the Laminar Boundary Layer in a Compressible Fluid," NACA TN 1115, Sep 1946

12. "Aerospace Research Capabilities," General Motors Corporation, GM DRL TR63-223, Apr 1964

13. Webb, W.H., Hromas, L. and Lees, L., "Hypersonic Wake Transition," AIAA Journal, Vol. 1, No. 3, Mar 1963

14. Clay, W.G., Labitt, M. and Slattery, R.E., "The Measured Transition from Laminar to Turbulent Flow and Subsequent Growth of Turbulent Wakes (U)," AMRAC Proceedings, Vol. X, Apr 1964

15. Hromas, L. and Lees, L., "Effect of Nose Bluntness on the Turbulent Hypersonic Wake," BSD-TDR-62-354. Oct 1962

16. Van Driest, E., Reproduced in "The Dynamics and Thermodynamics of Compressible Fluid Flow," Vol. II, Shapiro, A. H., Ronald Press, 1954

17. Romig, M. F., "Conical Flow Parameters for Air in Dissociation Equilibrium," CONVAIR Res. Rept. 7, May 1960

DISTRIBUTION LIST
for Analysis Reports on the
HYPERVELOCITY RANGE RESEARCH PROGRAM

Recipient	Copy No.
Director Advanced Research Projects Agency Washington 25, D. C. 20315	
ATTN: F. Koether	1 – 3
ATTN: Dr. B. Fisher	4
ATTN: C. McLain	5
ATTN: Major J. Kiernan	6
Aerojet-General Corporation P.O. Box 296 Azusa, California	
ATTN: Technical Library	7
Aeronutronics Division, Ford Motor Co. Ford Road Newport Beach, California	
ATTN: Technical Information Services	8
Aerospace Corporation 2400 E. El Segundo Blvd. El Segundo, California	
ATTN: Manager of Penetration Aids	9
Aerospace Corporation P.O. Box 95085 Los Angeles 45, California	
ATTN: J. Logan	10
Aerospace Corporation San Bernardino, California	
ATTN: Mr. R. Fowler	11
ATTN: Mr. Howard Meyers	12 – 41
Avco-Everett Research Laboratory 2385 Revere Beach Parkway Everett 49, Massachusetts	
ATTN: Dr. Bennett Kivel	42
ATTN: Technical Library	43
Avco Corporation Research and Advanced Development Division Wilmington, Massachusetts	
ATTN: Dr. A. Pallone	44
ATTN: Dr. W. E. Gibson	45
ATTN: Dr. J. Ekerman	46
ATTN: Dr. Wentink	47
ATTN: Dr. H. DeBolt	48
ATTN: Technical Library	49

Recipient	Copy No.
U.S. Air Force Ballistic Systems Division AF Unit Post Office Los Angeles 45, California	
ATTN: Major R. Fowler/WDTVP	50
ATTN: Major W. Levy	51
ATTN: Lt. K.G. Jefferson	52
Bell Telephone Laboratories Murray Hill, New Jersey	
ATTN: Dr. I. Pelech	53
ATTN: Dr. S.P. Morgan	54
ATTN: Dr. S.J. Buchsbaum	55
USAF Cambridge Research Laboratories Laurence Hanscom Field Bedford, Massachusetts	
ATTN: CRRELR, Stop 29	56
Director USAF Office of Scientific Research Washington 25, D.C.	
ATTN: Mechanics Division/ Major Terrell	57
Director Ames Research Center Moffett Field, California	
ATTN: H. Allen	58
Applied Physics Laboratory The Johns Hopkins University 8621 Georgia Avenue Silver Spring, Maryland	
ATTN: G. Seielstad	59
Applied Physics Laboratory Sylvania Elec. Products Waltham, Massachusetts	
ATTN: R. Row	60
Armour Research Foundation 10 W. 35th. Street Chicago 16, Illinois	
ATTN: Fluid Dynamics Research Division	61

DISTRIBUTION LIST (continued)

Recipient	Copy No.
Commanding General U.S. Army Air Defense Command Colorado Springs, Colorado ATTN: Advanced Projects Division, G-3	62
Commanding General U.S. Army Ballistics Research Laboratories Aberdeen Proving Ground, Maryland ATTN: C.H. Murphy	63
ATTN: B.J. Karpov	64
Commanding General U.S. Army Elec. and Communications Command Research and Development Fort Monmouth, New Jersey	65
Commanding General U.S. Army Materiel Command Washington 25, D.C.	66
Commanding General U.S. Army Missile Command Redstone Arsenal, Alabama 35809 ATTN: AMSMI-RB	67
ATTN: AMSMI-RRX	68
ATTN: AMSMI-RNR	69 – 73
Commanding General U.S. Army Materiel Command Redstone Arsenal, Alabama ATTN: AMCPM-ZER-R	74
Security Office, Army Missile Command Pacific Field Office Box 56, Navy 824 c/o FPO, San Francisco, California ATTN: Dr. S. Edelberg	75
Commanding General U.S. Army Research and Development Washington 25, D.C. ATTN: Intl. Division	76
ATTN: Physical Sciences Division	77
Commanding Officer U.S. Army Signal Missile Support Agency White Sands Missile Range, New Mexico ATTN: SIGWS-MM-1	78
ATTN: MEW	79
U.S. Army Technical Intelligence Agency Arlington Hall Station Arlington 12, Virginia ATTN: ORDLI	80
ARO, Inc. von Karman Facility Tullahoma, Tennessee ATTN: J. Lukasiewicz	81
Air Force Ballistic Systems Division Norton Air Force Base, California 92409 ATTN: Major Thurmond Deloney – BSYST	82
Special Projects Office Department of the Navy Washington 25, D.C. ATTN: Martin Bloom, SP-272	83
Barnes Engineering Company 30 Commerce Road Stamford, Connecticut ATTN: H. Yates	84
Battelle Memorial Institute 505 King Avenue Columbus 1, Ohio ATTN: Battelle-DEFENDER	85
Bell Telephone Laboratories, Inc. Whippany, New Jersey ATTN: C.W. Hoover, Room 2B-105	86
ATTN: C.E. Paul	87
ATTN: John McCarthy	88
Bendix Corporation Systems Division 3300 Plymouth Road Ann Arbor, Michigan ATTN: Systems Analysis and Math Dept.	89
ATTN: Flight Sciences Department	90
Boeing Airplane Company P.O. Box 3707 Seattle, Washington ATTN: Org. 2-5732, J. Klaimon	91
Brown Engineering Company Huntsville, Alabama ATTN: Technical Library	92

DISTRIBUTION LIST (continued)

Recipient	Copy No.
California Institute of Technology Pasadena, California ATTN: Prof. L. Lees	93
Central Intelligence Agency 2930 E Street, N.W. Washington, D.C. ATTN: OCR Standard Distribution	94 – 96
Communication and Propagation Laboratory Stanford Research Institute Menlo Park, California ATTN: Mr. Ray L. Leadabrand, Head, Propagation Group	97
ATTN: Dr. Carson Flammer	98
University of Michigan Willow Run Laboratories P.O. Box 2008, Ann Arbor, Michigan ATTN: BAMIRAC/B.R. George	99
Cornell Aeronautical Laboratory 4455 Genesee Street Buffalo 21, New York ATTN: J. Lotsof	100
ATTN: W. Wurster	101
ATTN: Applied Physics Dept.	102
Defense Research Corporation 6300 Hollister Avenue, Goleta, California ATTN: W. Short	103
Director Electromagnetic Warfare Laboratory Wright-Patterson Air Force Base Dayton, Ohio ATTN: ASRN/W. Bahret	104
Electro-Optical Systems, Inc. 300 N. Halstead Street Pasadena, California ATTN: R. Denison	105
General Applied Sciences Laboratories Merrick and Stewart Avenues Westbury, Long Island, New York ATTN: R. Byrne	106
General Dynamics Corporation Astronautics Division, P.O. Box 1128 San Diego, California 92112 ATTN: Library and Information Services (128-00)	107
General Electric Company Re-entry Vehicles Division 3198 Chestnut Street Philadelphia, Pennsylvania ATTN: L.I. Chasen, Room 3446	108
Geophysics Corporation of America Burlington Road Bedford, Massachusetts	109
Heliodyne Corporation 2365 Westwood Blvd. Los Angeles 64, California ATTN: S. Feldman	110
Institute for Defense Analyses 1666 Connecticut Avenue, N.W. Washington 9, D.C. ATTN: Dr. J. Menkes	111
ATTN: Dr. L. Biberman	112
ATTN: Dr. R. Fox	113
ATTN: Dr. J. Martin	114
ATTN: Mr. D. Katcher, JASON Library	115
ATTN: Mr. H. Wolfhard	116
Polytechnic Institute of Brooklyn 333 Jay Street Brooklyn, New York ATTN: Dr. N. Marcuvitz	117
Jet Propulsion Laboratory 4800 Oak Grove Drive Pasadena, California ATTN: H. Denslow	118
Kaman Nuclear Division Colorado Springs, Colorado ATTN: A. Bridges	119
Director Langley Research Center Langley Field, Virginia ATTN: W. Erickson	120
ATTN: R.L. Trimpi	121
Lockheed Corporation Missiles and Space Division Sunnyvale, California ATTN: Ray Munson	122
Special Projects Office Bureau of Weapons Munitions Building, Washington, D.C. ATTN: Cdr. Julian SP-25	123

DISTRIBUTION LIST (continued)

Recipient	Copy No.
Martin Aircraft Company Orlando, Florida ATTN: J. Mays	124
Director Marshall Space Flight Center Huntsville, Alabama ATTN: M-AER-TS	125
Massachusetts Institute of Technology Lincoln Laboratory P.O. Box 73 Lexington 73, Massachusetts ATTN: M. Herlin ATTN: R. Slattery ATTN: V. Guethlen	126 127 128
Chief U.S. Navy Bureau of Weapons Washington 25, D.C. ATTN: RMWC-322	129
Chief of Naval Operations Washington 25, D.C. ATTN: OP-07T10	130
Commander U.S. Naval Ordnance Laboratory White Oak, Silver Springs, Maryland ATTN: Technical Library	131
Director U.S. Naval Research Laboratory Washington 25, D.C. ATTN: Code 2027	132
New York University Department of Aero Engineering University Heights New York 53, New York ATTN: L. Arnold	133
North American Aviation Space and Information Systems Division 12214 Lakewood Blvd. Downey, California ATTN: E. Allen	134
Princeton University Princeton, New Jersey ATTN: Prof. E. Frieman ATTN: Prof. S. Bogdonoff	135 136
Purdue University School Aero and Engineering Sciences LaFayette, Indiana ATTN: I. Kvakovsky	137
Radio Corporation of America Missiles and Surface Radar Division Moorestown, New Jersey	138
The Rand Corporation 1700 Main Street Santa Monica, California ATTN: Library	139
Raytheon Manufacturing Company Missile Systems Division Bedford, Massachusetts ATTN: I. Britton, Librarian	140
Rome Air Development Center Griffiss Air Force Base Rome, New York ATTN: P. Sandler	141
The Martin Company Aerospace Division, Mail No. T-38 P.O. Box 179, Denver, Colorado 80201 ATTN: R.E. Compton, Jr.	142
Space Technology Laboratories, Inc. 1 Space Park Redondo Beach, California ATTN: Leslie Hromas	143
The Warner and Swasey Company Control Instrument Division 32-16 Downing Street Flushing 54, New York	144
University of California San Diego, California ATTN: Prof. N.M. Kroll	145
University of California Lawrence Radiation Laboratory Livermore, California ATTN: C. Craig	146
Scientific and Technical Information Facility P.O. Box 5700 Bethesda, Maryland ATTN: NASA Representative (SAK/DL-639)	147, 148

DISTRIBUTION LIST (concluded)

Recipient	Copy No.
General Electric Company Re-entry Systems Department Missile and Space Division P.O. Box 8555 Philadelphia, Pennsylvania ATTN: Mr. H.W. Ridyard	149
University of Michigan Radiation Laboratory 201 Catherine Ann Arbor, Michigan ATTN: R.J. Leite	150
Valley Forge Space Technical Center General Electric Company P.O. Box 8555 Philadelphia 1, Pennsylvania ATTN: J. Farber ATTN: K. Wau	151 152
Director Weapons Systems Evaluation Group Pentagon, Room 1E-800 Washington 25, D.C. 20315	153
U.S. Army Liaison Office Canadian Armament Research and Development Establishment P.O. Box 1427 Quebec, P.Q., Canada ATTN: Lt. Col. E.W. Kreischer	154
*Commanding General U.S. Army Missile Command Redstone Arsenal, Alabama 35809 ATTN: SMIDW-BI(C)	155
United Aircraft Corporation Research Laboratories East Hartford, Connecticut ATTN: Dr. R. Meyerand	156
Monsanto Research Corporation Boston Laboratory Everett, Massachusetts 02149 ATTN: Dr. L. Gilman	157
Defense Documentation Center Cameron Station Alexandria, Virginia	158 – 177
Capt. L.L. Schoen, USAF USAF Technical Representative c/o GM Defense Research Laboratories	178
GM Defense Research Laboratories	179 and above

* Unclassified reports only.

Additional Distribution for Semiannual Reports only:

Office of Naval Research Department of the Navy Washington 25, D.C.	
ATTN: Dr. S. Silverman, Science Director	1 copy
ATTN: Dr. F. Isakson, Physics Branch	1 copy
ATTN: Mr. M. Cooper, Fluid Dynamics Branch	1 copy

GM Defense Research Laboratories, General Motors Corp., Santa Barbara, California

BODY SHAPE EFFECTS ON AXISYMMETRIC WAKES by L. N. Wilson, TR64-02K, 40 pp. inc. 20 illus., 17 refs.

Experimental measurements have been made of the distance of transition to turbulence of the wake behind hypersonic spherical and blunted-cone models. The transition process was found to be markedly different between blunt and slender body flows, the transition occurring rather abruptly behind blunt bodies and being extended over many body diameters for slender bodies. In all cases, the transition distances were independent of body size and flight speed. The correlations were found to break down at high Reynolds numbers where turbulence originated at the

(Unclassified)

1. Hypervelocity projectiles – Test results
2. Hypervelocity projectiles – Wake
3. Schlieren photography – Applications
4. Guided missile – Detection

I. DA-01-021-AMC-11359(Z)
II. TR64-02K
III. Wilson, L. N.

(Descriptors) Hypervelocity projectiles, Wake,

GM Defense Research Laboratories, General Motors Corp., Santa Barbara, California

BODY SHAPE EFFECTS ON AXISYMMETRIC WAKES by L. N. Wilson, TR64-02K, 40 pp. inc. 20 illus., 17 refs.

Experimental measurements have been made of the distance of transition to turbulence of the wake behind hypersonic spherical and blunted-cone models. The transition process was found to be markedly different between blunt and slender body flows, the transition occurring rather abruptly behind blunt bodies and being extended over many body diameters for slender bodies. In all cases, the transition distances were independent of body size and flight speed. The correlations were found to break down at high Reynolds numbers where turbulence originated at the

(Unclassified)

1. Hypervelocity projectiles – Test results
2. Hypervelocity projectiles – Wake
3. Schlieren photography – Applications
4. Guided missile – Detection

I. DA-01-021-AMC-11359(Z)
II. TR64-02K
III. Wilson, L. N.

(Descriptors) Hypervelocity projectiles, Wake,

GM Defense Research Laboratories, General Motors Corp., Santa Barbara, California

BODY SHAPE EFFECTS ON AXISYMMETRIC WAKES by L. N. Wilson, TR64-02K, 40 pp. inc. 20 illus., 17 refs.

Experimental measurements have been made of the distance of transition to turbulence of the wake behind hypersonic spherical and blunted-cone models. The transition process was found to be markedly different between blunt and slender body flows, the transition occurring rather abruptly behind blunt bodies and being extended over many body diameters for slender bodies. In all cases, the transition distances were independent of body size and flight speed. The correlations were found to break down at high Reynolds numbers where turbulence originated at the

(Unclassified)

1. Hypervelocity projectiles – Test results
2. Hypervelocity projectiles – Wake
3. Schlieren photography – Applications
4. Guided missile – Detection

I. DA-01-021-AMC-11359(Z)
II. TR64-02K
III. Wilson, L. N.

(Descriptors) Hypervelocity projectiles, Wake,

GM Defense Research Laboratories, General Motors Corp., Santa Barbara, California

BODY SHAPE EFFECTS ON AXISYMMETRIC WAKES by L. N. Wilson, TR64-02K, 40 pp. inc. 20 illus., 17 refs.

Experimental measurements have been made of the distance of transition to turbulence of the wake behind hypersonic spherical and blunted-cone models. The transition process was found to be markedly different between blunt and slender body flows, the transition occurring rather abruptly behind blunt bodies and being extended over many body diameters for slender bodies. In all cases, the transition distances were independent of body size and flight speed. The correlations were found to break down at high Reynolds numbers where turbulence originated at the

(Unclassified)

1. Hypervelocity projectiles – Test results
2. Hypervelocity projectiles – Wake
3. Schlieren photography – Applications
4. Guided missile – Detection

I. DA-01-021-AMC-11359(Z)
II. TR64-02K
III. Wilson, L. N.

(Descriptors) Hypervelocity projectiles, Wake,

recompression region. A method of using the distance to transition in clean wakes to discriminate between blunt and slender bodies is outlined.

Turbulence, Fluid flow, Blunt bodies, Spheres, Measurement, Re-entry vehicles, Atmosphere entry, Guided missile detection, Schlieren photography, Lasers, Boundary layer, Ablation

recompression region. A method of using the distance to transition in clean wakes to discriminate between blunt and slender bodies is outlined.

Turbulence, Fluid flow, Blunt bodies, Spheres, Measurement, Re-entry vehicles, Atmosphere entry, Guided missile detection, Schlieren photography, Lasers, Boundary layer, Ablation

recompression region. A method of using the distance to transition in clean wakes to discriminate between blunt and slender bodies is outlined.

Turbulence, Fluid flow, Blunt bodies, Spheres, Measurement, Re-entry vehicles, Atmosphere entry, Guided missile detection, Schlieren photography, Lasers, Boundary layer, Ablation

recompression region. A method of using the distance to transition in clean wakes to discriminate between blunt and slender bodies is outlined.

Turbulence, Fluid flow, Blunt bodies, Spheres, Measurement, Re-entry vehicles, Atmosphere entry, Guided missile detection, Schlieren photography, Lasers, Boundary layer, Ablation